Multi(4)-variate population balance modeling for shear aggregation in 3D space

Frédéric Gruy, Patrice Nortier

Multi(4)-variate Population Balance Modeling for Shear Aggregation in 3D space

Frédéric Gruy (*) and Patrice Nortier

Mines Saint-Etienne, Univ Lyon, CNRS, UMR 5307 LGF, Centre SPIN

F - 42023 Saint-Etienne France

* corresponding author

gruy@emse.fr

0033477420202

Abstract: shear aggregation of micrometric particles is an important phenomenon occurring in agitated chemical reactors. The resulting clusters of particles are porous and more or less elongated. It has previously been proved that the equivalent ellipsoid computed from the inertia tensor describes well the colliding clusters [F.Gruy and P. Nortier « Statistics about collisions of ellipsoids under shear flow » Colloids and Surfaces A: Physicochemical and Engineering Aspects, 558(2018)250-262]. The aim of the current paper is to consider chosen kinetic and morphological aspects of the complete aggregation dynamics. Monte Carlo simulations are used as a means of investigation. Four representations of the collision event have been compared: the classical collision of oriented clusters of sphere (A), the collision of oriented equivalent ellipsoids (B), the orientation-averaged collision of equivalent ellipsoids (C), the use of approximate expressions for C (D). For each case, the probability density functions of various morphological parameters of the cluster population are calculated as a function of the time. The comparison of the generated data shows that the approximate expressions for the aggregation kernel and the ellipsoid parameters allow for fast and representative simulations of the shear aggregation of suspensions.

Keywords: aggregation, inertia tensor, equivalent ellipsoid, Monte Carlo simulation, population balance

Nomenclature

$\vec{A}$	vector between the centres of mass of two particles ($\vec{A} = \overrightarrow{C_1C_2}$)
a	semi-major axis of ellipsoid
b,c	semi-minor axis of ellipsoid
C	centre of mass of particle
d	estimate of A
D_f	fractal dimension
$\underline{\underline{D_I}}$	diagonalized inertia tensor
$\underline{\underline{D_{I,m}}}$	diagonalized inertia tensor after averaging
f	solid volume fraction in the cluster
$\underline{\underline{f_{12}}}$	diagonal tensor (Eq.16)
F_{ab},F_{ac},F_{bc}	6x6 matrices (Eq.18)
$\underline{\underline{I}}$	inertia tensor of the particle
k	prefactor of the fractal law
k_{12}	contribution to K_{12}
K_{12}	kernel of aggregation
L	penetration length
M	particle mass
n	probability density

nb particle number in the MC simulation

n_c population density in the suspension

N number of primary particles per aggregate

N_r number (MC runs) of elementary collision events to describe the aggregation event between two given clusters

N_t number (MC runs) of aggregation events

N_a number of complete aggregation processes (reproducibility)

r_i random number within the range [0; 1]

R_g gyration radius

S_p projected area

t dimensionless time

t_f time corresponding to the beginning of the runaway growth

T physical time

U fitting parameter (case D)

v particle volume

V MC box volume

X, X_0 particle concentration in the suspension at time t and t=0

W fitting parameter (case D)

$\vec{x}$ position vector of particle

x,y,z space coordinates

Greek letters

δ Kronecker symbol $\delta_{k,l}=1$ if $k=l$; $\delta_{k,l}=0$ if $k\neq l$

ϕ_{SLC},ϕ_{LC} ratio of the LC or SLC mass to the particle set mass

$\phi_i = M_i/\left(M_1+M_2\right)$

ϕ solid volume fraction in the suspension

$\varphi(\eta,\tau)$ dimensionless population density

(η,τ) dimensionless variables

$\dot{\gamma}$ shear rate

κ permeability

ρ mass density

Ω Euler angle

Superscript

(i) for tensor (particle *i*)

Subscript

$\underline{\underline{X}}$ tensor *X*

app approximate

eq equivalent

i for scalar or vector (particle *i*)

i,k *k* component of vector (particle *i*)

k,l *k,l* element of the tensor or matrix

m mean value

LC largest cluster

SLC second largest cluster

symbol

< > average

1. Introduction

Multiphase flows appear in many industrial processes: bubbly flow, emulsion, aerosol, suspension. Disperse phase may be composed of different kind of particles: bubbles, drops, crystals or amorphous grains. Due to phenomena such as nucleation, growth, coalescence or aggregation, the number, the size and the shape of particles are changing with time. The dynamics of the disperse phase may be modelled by a means of the population balance modelling (PBM). The key point of the modelling is the choice of the morphological or geometrical descriptors (MD) that constitute the internal parameters of the population balance equation (PBE). The simplest analysis of disperse phase considers the particle as a sphere having equal amounts of matter; the only MD is the radius of the sphere and the PBE is monovariate [1]. Since the two past decades, PBM considers particles depicted by several MD's: the PBM is called multivariate (see, for instance, [2]). The choice of the MD is often made based on physical arguments fitted with the studied problem. However, the selection of MD has to obey some mathematical rules. Shape of particles may be divided into two classes: convex (sphere, ellipsoid, polyhedron) or non-convex (cluster of convex particles, erythrocytes …). The theory of Minkowski Functionals provides the rigorous framework for such parameter set. Mecke et al. [3-4] have applied the integral geometry in various fields of physics. Scalar Minkowski Functionals of a convex or non-convex particle in a 3D space are the volume, the surface area, the mean curvature and the Gaussian curvature averaged over the surface of the particle. Tensorial Minkowski Functionals (TMF) are an extension of the scalar ones. Recently, Essadki et al. [5] have modelled the atomization of a fuel with air from the exit of the injector nozzle to the combustion chamber; the two-phase flow changed from a separated flow to a disperse phase in a continuous medium. In particular the dynamics of the disperse phase is described by a means of a multivariate population balance equation; they

have considered a new phase-space including the particle surface area, the averages of the mean curvature, the Gauss curvature and the fuel-air interface velocity over the particle surface. The PBE includes terms for time evolution of new variables and for coalescence and fragmentation of droplets as well. The evolution equations for the curvatures in PBE are based on the work of Drew [6].

Pure aggregation of solid particles has to be treated differently than the coalescence of droplets; The curvatures of primary particles and aggregates are not the most relevant variables associated with the dynamics of aggregation. Aggregation of particles in a suspension is due to the binary collisions between two particles. The resulting aggregate or cluster is a branched and porous object consisting of primary particles, usually considered as identical. Most often, the morphology of the cluster is described by using the fractal theory: the cluster is built by successive attachments of smaller entities which leads to a hierarchical structure. In colloid science, the cluster is essentially defined by the radius of the primary particle, its number of primary particles and the fractal dimension D_f [7]. The last quantity is a real number within the 1-3 range which is the exponent in the power law, linking the number of primary particles and the gyration radius R_g. Even if the fractal hypothesis was successful in describing the dynamics of aggregation, the fractal dimension is not the only relevant morphological parameter. It has been proved [8] that the aspect ratio of the aggregate is a major parameter for the dynamics of aggregate collisions.

As this paper is concerned by the modelling of pure shear aggregation, we remind some non-exhaustive literature focused on the topic. Some authors consider shear aggregation as a ballistic aggregation. However, other authors dispute this point (see Elimelech et al. ([1], p.182)) that can be involved in the following:

- Hentschel [9] recalls that Meakin showed that D_f=1.91 for 3-D ballistic cluster-cluster aggregation. He added that the anisotropy factor (as the ratio of the two largest

principal gyration radii) is equal to 2. From dimensional arguments, Hentschel found D_f=1.80; This value does not depend on the collision mechanism and is consistent with a weak interpenetration of clusters and an anisotropy factor equal to 2.

- Potanin [10] has found a D_f value equal to 1.98.
- Torres et al. [11] have, for instance, performed simulations of 3-D shear aggregation. They found a fractal dimension value equal to 1.83 and they observed the non-spherical shape of the aggregate. Moreover, they have calculated the gyration tensor (normalized by the square of the gyration radius) for clusters with a number N of primary particles smaller than 4100. They have observed that the semi-axes ratio of the equivalent ellipsoid were a/b=1.94 and a/c=3.1, whatever the origin of the particle collision (Brownian motion, shear flow, elongation flow).
- Frungieri and Vanni [12] have simulated the cluster-cluster aggregation by considering weak Van der Waals interaction and tangential interaction; in the absence of tangential interaction, the primary particles in the cluster are free to slide and roll over each other; therefore, a compaction of the cluster can be observed early. Tangential interaction strongly hinders the restructuring and leads to a more open structure. Corresponding clusters look like isostatic ones, where contact and bond between colliding clusters is achieved between two primary particles leading to a frozen structure. The fractal dimension was found equal to 1.88. The authors defined an aspect ratio from the parameters of the equivalent ellipsoid of the cluster and computed the corresponding probability density function (pdf) for the particle population.
- Pranami et al.[13] studied the anisotropy of clusters with prescribed fractal dimension which was found to satisfy well the scaling relation. The authors selected two shape anisotropy parameters based on the principal moments of inertia. They computed the

two pdf's for different N values where N is the number of primary particles in the cluster; The results showed that the pdf curves overlap irrespective of the N-value.

Gyration radius and aspect ratio of the aggregate may be defined from its inertia tensor. The shape of the convex hull of aggregates may be approximated by an ellipsoid. Inertia tensor is a quantity similar to TMF and a more popular concept among physicists than the Minkowski functionals. Therefore, inertia tensor may be used as morphological descriptor for particles.

Gruy laid the foundations of a new modelling method for the aggregation based on the inertia tensor and the equivalent ellipsoid [14]. This has been illustrated in the simplest case: the 2D-aggregation of equivalent ellipses of 2D-clusters under shear flow. We have also determined the collision dynamics and the parameters of the resulting equivalent ellipsoid for ellipsoids and 3D-clusters [15]. More specifically, some empirical expressions aiming at accelerating the simulations of particle population dynamics have been proposed. Therefore the collision act as defined by Gmachowski [16] is completely described in [15]: each particle is described by its mass content and the three semi-axes of the equivalent ellipsoid. The aim of this paper is to consider the complete dynamics of the population of particles by applying our previous results about the elementary aggregation act. Monte Carlo Simulations (MCS) will be used to solve the multivariate population balance.

Section 2 is dedicated to the methods: the theoretical elements corresponding to the collision of two clusters and the algorithms for Monte Carlo Simulation. Section 3 contains the results for the aggregation dynamics of the entire population. Section 4 discusses the results and concludes the paper.

2. Methods

2.1. Aggregation act

The aggregation dynamics of a suspension is studied by a means of a population balance. The particles are described by their internal parameters, the morphological parameters included. The additivity of the parameters of two colliding particles, denoted by 1 and 2, is an important property needed for a concise writing of the population balance. This property is verified by the mass or the matter volume:

$$M_{1+2} = M_1 + M_2 \tag{1}$$

It is not the case for the common morphological descriptors, e.g. aspect ratio, roundness, …, that have not been intended for studying aggregation. However, this is almost the case for the inertia tensor if it is evaluated about the centre of mass of the resulting cluster. We recall hereafter how to consider the inertia tensor in the aggregation act. Details may be found in [14].

Let us consider two objects with the inertia tensors $\underline{\underline{I}}^{(1)}$ and $\underline{\underline{I}}^{(2)}$, each one evaluated about its own centre of mass C_i. Then the inertia tensor of the object resulting from the collision of two smaller objects with the centres of mass separated by $\vec{A} = \overrightarrow{C_1C_2}$ obeys the equation [17]:

$$I_{kl}^{(1+2)} = I_{kl}^{(1)} + I_{kl}^{(2)} + \frac{M_1 M_2}{M_1 + M_2}\left(\vec{A}^2 \delta_{kl} - A_k A_l\right) \tag{2}$$

One defines the equivalent ellipsoid as the real ellipsoid having the same diagonalized inertia tensor as the object (1, 2 or 1+2). Each equivalent ellipsoid has an orientation defined by the Euler angles Ω_i. The solid volume of primary particles is smaller than the geometrical volume of the equivalent ellipsoid. It is assumed that the vector $\vec{A} = \overrightarrow{C_1C_2}$ is such as the equivalent ellipsoids of the two colliding objects/clusters are tangent in the sense of the geometry. This hypothesis is not trivial and will be discussed later on: as the radius of gyration of fractal aggregates is smaller than the geometrical size, one may expect that the distance between the centres of the two colliding equivalent ellipsoids will be shorter than the previously assumed one.

The equivalent ellipsoid of the resulting object is obtained from the diagonalization of the tensor $\underline{\underline{I}}^{(1+2)}$; the corresponding tensor is denoted by $\underline{\underline{\underline{\underline{D}}}}_I^{(1+2)}$. Then, the mathematical treatment of a collision event of two clusters, which are approximated as ellipsoids, will follow the sequence:

1. transform ellipsoid to inertia tensors for defined orientation:

$\left(a^{(i)}, b^{(i)}, c^{(i)}\right) \rightarrow \underline{\underline{\underline{\underline{D}}}}_I^{(i)} \xrightarrow{\Omega_i} \underline{\underline{I}}^{(i)}$ with *i=1,2*

2. compute new inertia tensor (Eq.2):

$\underline{\underline{I}}^{(1)} + \underline{\underline{I}}^{(2)} \rightarrow \underline{\underline{I}}^{(1+2)}$

3. determine the geometric parameters of the equivalent ellipsoid:

$\underline{\underline{I}}^{(1+2)} \rightarrow \underline{\underline{\underline{\underline{D}}}}_I^{(1+2)} \rightarrow \left(a^{(1+2)}, b^{(1+2)}, c^{(1+2)}\right)$

$a^{(1+2)}, b^{(1+2)}, c^{(1+2)}$ are the semi-axis lengths of the equivalent ellipsoid. This sequence can be repeated when modelling the aggregation phenomenon.

In practice, aggregation involves a large number of particles; a sub-set of particles has the same morphological characteristics, but with different orientations. Therefore, the description of a collision between two objects with different morphological parameters needs to be averaged over all the possible orientations of the two objects $\left\langle \underline{\underline{\underline{\underline{D}}}}^{(1+2)} \right\rangle_{(\Omega_1, \Omega_2)}$. The calculations of mean values $\langle \ \rangle_{\Omega_i}$ are performed over all the orientations. The average is applied to $\underline{\underline{\underline{\underline{D}}}}_I^{(1+2)}$.

This procedure has been selected for the following reason:

Specifying the orientation of the ellipsoids for each collision add a unit vector, i.e. its components, into the set of internal variables describing the particle. In order to reduce the number of internal variables an averaging over orientations and relative positions is done. Hence, a particle is characterized by only its mass and the lengths of the ellipsoid semi-axes.

This will be particularly important when solving the corresponding population balance equation.

The orientations of the two colliding objects are assumed non-correlated, i.e. the hydrodynamic resistance between two particles moving towards each other is not taken into account. The orientation angle distribution of a particle in a fluid depends on its shape and on the flow field. The relative position of the centres of mass at impact $\vec{A} = \overrightarrow{C_1C_2}$ depends on the orientations and the initial relative position of the two objects, and on the mechanism of collision. Finally the inertia tensor of the resulting cluster after the collision of two smaller objects is:

$$\underline{\underline{D_{I,m}^{(1+2)}}} = \left\langle \left\langle \underline{\underline{D_I^{(1+2)}}} \right\rangle_{(C_1,C_2)} \right\rangle_{(\Omega_1,\Omega_2)} \tag{3}$$

m refers to the mean value of $\underline{\underline{D_I^{(1+2)}}}$; the average $\langle\ \rangle_{(C_1,C_2)}$ is performed over all the possible loci of the two centres of mass of the particles in contact.

The two main mechanisms, so-called perikinetic and orthokinetic, for aggregation are characterized by different kinetic constants or kernels [1]. From a geometrical point of view:

- In the case of perikinetic aggregation, two particles moving thanks to Brownian motion have the same collision probability whatever the relative angular position.
- In the case of orthokinetic aggregation, the probability of encounter is higher as the two particles are offset to the side in the shear flow: The relative velocity of the colliding particles is proportional to the distance between the corresponding parallel streamlines; for instance, the impact of particles moving on the same streamline is unlikely.

Thus, one may write:

$$\underline{\underline{D_{I,m}^{(1+2)}}} = \left\langle \left\langle \underline{\underline{D_I^{(1+2)}}} \right\rangle_{(C_1,C_2)} \right\rangle_{(\Omega_1,\Omega_2)} = \left\langle \int_{\Sigma(\Omega_1,\Omega_2)} \underline{\underline{D_I^{(1+2)}}} dk_{12} \right\rangle_{(\Omega_1,\Omega_2)} / K_{12} \tag{4}$$

K_{12} consistently denotes the aggregation kernel. dk_{12} is the contribution of an infinitesimal interception or collision area to the kernel. One performs the sum over all the collision area. The whole collision area, that depends on the orientations of the two particles, is denoted by $\Sigma(\Omega_1, \Omega_2)$.

As a consequence, the kernel obeys the relation:

$$\left\langle \int_{\Sigma(\Omega_1,\Omega_2)} dk_{12} \right\rangle_{(\Omega_1,\Omega_2)} = K_{12} \tag{5}$$

Therefore the geometrical properties of the average equivalent ellipsoid will be deduced from $\underline{\underline{D_{I,m}^{(1+2)}}}$ and will be denoted by $a_m^{(1+2)}, b_m^{(1+2)}, c_m^{(1+2)}$. The averaging step is performed by the MC method based on repeating N_r times the elementary collision event.

This approach is applied to the case of the orthokinetic aggregation. One considers a shear flow in a three-dimensional space ($\vec{k}$ is the unit vector along the flow direction, the unit vector $\vec{j}$ corresponds to the velocity gradient, $\vec{i} = \vec{j} \wedge \vec{k}$).

$$dk_{12} = \dot{\gamma} \left| \overrightarrow{C_1C_2} \bullet \vec{j} \right| dS_p \tag{6}$$

where $\dot{\gamma}$ is the shear rate, dS_p is the element of area swept by the orthogonal projection along $\vec{k}$ of $\overrightarrow{C_1C_2}$ in the plane $\left(\vec{i}, \vec{j}\right)$. The orientation angle distribution of a single ellipsoid is assumed uniform. As a reminder, the hydrodynamic resistance is neglected in this paper. These assumptions are discussed in [14-15].

Aggregation is a series of collisions between equivalent ellipsoids; each collision event or aggregation act corresponds to:

$$\left(M_1, D_{11}^{(1)}, D_{22}^{(1)}, D_{33}^{(1)}\right) + \left(M_2, D_{11}^{(2)}, D_{22}^{(2)}, D_{33}^{(2)}\right) \xrightarrow{K_{12}} \left(M_1 + M_2, D_{11}^{(1+2)}, D_{22}^{(1+2)}, D_{33}^{(1+2)}\right) \tag{7}$$

The subscript *m* is withdrawn from the diagonal elements of $\underline{\underline{D_{I,m}}}$ and the corresponding semi-axis lengths, considering that the equivalent ellipsoid has forgotten the memory of its construction.

The collision event may be rewritten as:

$$\left(M_1, a^{(1)}, b^{(1)}, c^{(1)}\right) + \left(M_2, a^{(2)}, b^{(2)}, c^{(2)}\right) \xrightarrow{K_{12}} \left(M_1 + M_2, a^{(1+2)}, b^{(1+2)}, c^{(1+2)}\right) \quad (8)$$

The colliding particle ((1) or (2)) may have any shape, e.g. sphere, needle, ellipsoid, aggregate…; its geometry properties are replaced by those of the equivalent ellipsoid. However, the resulting particle (1+2) will be only considered as an ellipsoid, i.e. the average equivalent ellipsoid; the real shape of the resulting particle will not be known. As a consequence, the complete aggregation process will consider a set of collisions between ellipsoids. Each particle, i.e. ellipsoid, is therefore defined by four internal variables.

2.2. Aggregation dynamics

A Monte-Carlo method has been selected to solve the population dynamics. One starts from a population consisting of a large number of primary particles; the probability to have a collision between any two particles is proportional to the corresponding kinetic constant (kernel) of aggregation. Hence, two objects are randomly selected by applying this probability distribution. Then its equivalent ellipsoid is calculated. The process is repeated until clusters, i.e. their equivalent ellipsoids, with a large number (N=10^4) of primary particles are built. At a given time, the population of clusters, i.e. equivalent ellipsoids, can be analysed: pdf (probability density function) of *N*, pdf of anisotropy parameters, fractal dimension ….

MCS for reaction set and aggregation have been introduced by Gillepsie [18]. He proposed three different algorithms. All these algorithms consider a number of particles that decreases as the aggregation proceeds; aggregation stops when there is only one cluster. The accuracy decreases during the simulation. Consequently, the initial number of particles must be very

large in order to reach a small number of large clusters and to study a few collision events between the large clusters. As the calculation of each MC step is proportional to the square of the number of particles, it is clear that this method becomes impracticable.

Smith and Matsoukas [19] have developed an algorithm based on one of the Gillepsie' algorithms, but working with a constant number of particles as the aggregation proceeds: at each aggregation event, the two colliding particles are replaced by the resulting cluster and a particle randomly chosen among particle population. Therefore, the initial number of particles can be much smaller. This algorithm is very efficient for Brownian aggregation, having a kernel showing a weak increase with the particle size. However, it works less efficiently when considering the shear aggregation for which the aggregation kernel is roughly proportional to the cubic particle size [1]. Ormel et al. [20] use another algorithm of Gillepsie, but working with a constant number of particles. This is very efficient for all aggregation kernels. It has been verified by comparing it with the analytical solutions of the stochastic coagulation equation [21]. Monte Carlo simulations are based on the stochastic coagulation equation. Smoluchowski equation is derived from the stochastic equation under certain assumptions. More specifically, Tanaka and Nakazawa [21] presented analytical solutions for the sum kernel, the homogeneity order of which is equal to one as the Smoluchowski kernel for sphere aggregation under shear flow [1].

The MC procedure used in this paper is the one proposed by Ormel. We recall the different steps of the algorithm:

We start with *nb* particles located in a box with volume *V*. For MC simulation, each particle is located in a numbered slot from one to *nb*. At each MC time-step, we calculate the following quantities:

$$C_{i,j} = K_{i,j} / V$$
$$C_i = \sum_{j=i+1}^{nb} C_{i,j} \; i = 1,...,nb-1 \qquad \text{(9a,b,c)}$$
$$C_t = \sum_{i=1}^{nb-1} C_i$$

$K_{i,j}$ is the aggregation kernel for particles *i* and *j*. $C_{i,j}$, C_i and C_t have no physical meaning and are mathematical intermediate variables.

- Selection of the two colliding particles *i* and *j* [18]

Let r_i be three random numbers within the range [0; 1].

- The time step Δt elapsed between two collisions is $\Delta t = -\ln(r_1)/C_t$ (10)

- The first collision partner will have the smallest *i* value such as $\sum_{k=1}^{i} C_k > r_2 C_t$ (11)

- The second collision partner will have the smallest *j* value such as $\sum_{k=i+1}^{j} C_{ik} > r_3 C_i$ (12)

  The result of the collision between *i* and *j* will be placed in the *i*-slot.

- Update [19,20]

  Another random number then determines which of the $nb - 1$ particles (excluding *j*) will be duplicated and this one is stored in the *j*-slot. Having modified the particle set, all of the *C*-s need to be updated. This entails only the subtraction/addition of the $C_{i,j}$ that have changed, not the re-computation of Eqs. (9). Moreover, this implies a rescaling of the simulated volume, *V*, such that the density of solids, $\sum_{i=1}^{nb} M_i / V$, remains constant. As $\sum_{i=1}^{nb} M_i$ increases with the time, the volume *V* of the box increases as well.

  The algorithm can then be repeated.

3. Results

In this section, several ellipsoid based modelling will be compared to the classical cluster formation for shear aggregation. For this purpose, one considers an initial monodisperse population of spheres (with radius 1 and with density 1). MCS will be performed with a constant number of particles, i.e. primary particles, clusters or ellipsoids, equal to 2000, whereas the number of time steps is chosen equal to 3000. The computational volume V of the box at time zero is chosen to be one. At a given time, i.e. after N_t time steps (N_t<3000), the population of particles will be analysed: pdf of N (number of primary particles inside the particle), pdf of anisotropy parameters as a/b and a/c, fractal dimension ….In the rest of the text, time t is dimensionless and is related to the real time T by the expression: $t = (3/4\pi)\dot{\gamma}\phi T$ where ϕ is the solid volume fraction in the suspension. The dimensionless time is frequently used when considering the shear aggregation and highlights some invariance properties of aggregating systems [22]. The value ranges of the physical parameters are within [10; 1000s^{-1}] for the shear rate and [10^{-5}; 10^{-2}] for the solid volume fraction in lab experiments and some industrial processes.

Therefore, we will begin by describing the formation of a population of clusters as the reference case.

3.1 Reference case (case A)

The aggregation of a monodisperse population of spheres leads to clusters of spheres. The aggregation act corresponds to the collision of two clusters. This collisional process is divided into the following steps (for details, see section 3 [15]) in MCS:

i) random orientation of the two clusters around their centres of mass

ii) choice of initial relative position and collision complying with the shear flow and stochastic processes

These steps can be repeated many (N_r) times or not repeated at all for a given two cluster set in order to extract information about the kinetic constant of collision and pdf of anisotropy parameters of the resulting clusters [15]. However, it is not possible to deduce an equivalent resulting cluster, i.e. defined by the coordinates of each constituent primary particle that would be statistically representative of all the effective collisions. For this reason only one collision ($N_r=1$) will be performed for the aggregation act between two given clusters; there is no average performed over orientation angle or relative position. On the other hand, the kinetic constant needed for MCS will be calculated by using Eq.5 with the parameters of the equivalent ellipsoids of the two clusters [15]. In this manner, the complete aggregation process will be a series of unique collision events between two given clusters. The complete aggregation process will be repeated N_a times in order to obtain an acceptable description. N_a has been fixed to 10 (It must be noted that this way of performing MCS is slightly different from this presented in sub-section 2.1). Two simulations with N_a=10 have been compared.

The figures 1A, 2A present the *N*-pdf for various times. Herein the *P*-pdf corresponding to the particle property *P* is defined as the number fraction of particle with *P* within the range [*P*,*P*+*dP*] divided by d*P*. As expected and showed in the table 1, the mean *N*-value is increasing with time. The two simulations lead to similar results; it will be also true for the figures 3A-6A. This indicates that 10 MCS run would be sufficient to get realistic data. The main feature is the presence of a large amount of small clusters (*N*<20) and of some very large particles. The figure 3A represents the largest cluster content versus dimensionless time. The latter increases dramatically and reaches very high value whereas the mean *N* value remains small; this is expected as the kernel of shear aggregation is proportional to the cubic particle sizes. Only fragmentation of large and loose particles may hinder this phenomenon. Therefore, without fragmentation or other size-limiting phenomenon, shear aggregation becomes catastrophic at a given time. This issue can be analysed by the method of Tanaka

and Nakazawa [21]: by comparing the stochastic and statistical coagulation equations, they proved that the statistical approach fails when a transition between aggregation and a runaway growth happens; at the same time, the mass content of the largest cluster strongly increases whereas the smaller clusters do not or decrease. This behaviour, i.e. the beginning of gelation, depends on the kernel expression and has been confirmed by Alfonso et al. [23-24] by using a statistical indicator. Figure 4A compares the change with time of the mass fraction of the largest cluster (ϕ_{LC}) and the second largest cluster (ϕ_{SLC}). It can be seen that the two corresponding mass fraction values deviate for ϕ_{LC}>0.1 as the time is running. ϕ_{LC}=0.3 seems to be the value beyond which the divergence occurs. The corresponding time t_f will be the ultimate instant for a relevant study of aggregation; as shown in the figure 3A, the corresponding cluster size, [10^3-10^4], is beyond the experimental value for the shear aggregation of micrometric particles [22, 25]. The t_f value is within the range 0.13-0.16. This wide value range is related to the stochastic nature of the gelation event [23-24]. The figures 5A, 6A present the *a/b*-pdf and *a/c*-pdf. *a*, *b* and *c* are the parameters of the equivalent ellipsoid deduced from the inertia matrix of the sphere clusters. The two pdf's are wide. *a/b* and *a/c* values are within the range [1; 5] and [1; 6] respectively. The peak at *a/b*=*a/c*=2.45 corresponds to the doublet of spheres [15]. Pdf's do not change with time for the time value larger than 0.09 (N_t>1000).

The gyration radius of a cluster consisting of *N* spheres with radius equal to one obeys the relation [7]:

$$R_g = \sqrt{\sum_{i=1}^{N} \vec{x}_i^{\,2} / N + 3/5} \qquad (13)$$

where the position vector of the sphere *i* is taken from the centre of mass of the cluster to the centre of the sphere. Considering the whole cluster population, we may draw the gyration radius versus *N* for various times. As an example, the Figure 7a shows such data for a given

time (t=0.136). We observe that the gyration radius versus N obeys a power law, i.e. $R_g = kN^{1/D_f}$, like for fractal-like aggregates [7]. The prefactor k and the fractal dimension D_f may be obtained from a least square optimization algorithm applied to the cluster set (N>3). The Table 2 reports them for each time: the prefactor value is about 0.9 whereas the fractal dimension is about 2. A slight drift with the time can be observed; however its amplitude is much smaller than the one due to the restructuring of clusters.

Following Friedlander and Wang [26], the population density $n_c(v,t)$ of an aggregating suspension may be transformed by using the new variables:

$$\begin{aligned} n_c(v,t) &= X(t)^2 / \phi \varphi(\eta,\tau) \\ \eta &= Xv/\phi \\ \tau &= \left(X / X_0\right)^2 \end{aligned} \qquad (14)$$

v is the volume of the particle. X and X_0 are the total concentrations of particle at time t and 0, respectively. φ is a dimensionless distribution function. For certain aggregation kernels and for long times, the function $\varphi(\eta,\tau)$ tends to the self-preserving function $\varphi_{as}(\eta)$. As a consequence, when $\phi X(t)^{-2} n_c(v,t)$ is plotted against Xv/ϕ , the size distribution curves corresponding to various times become a single curve. This has been previously used for the study of the shear aggregation [27]. When applying this transformation to the data generated from the constant-number Monte Carlo simulations, we draw $n(N,t) < N >$ against $N / < N >$ for various times. The figure 7b contains such data for the case A. It can be observed that a self-preserving pdf is rapidly reached (t>0.03; N_t>300).

3.2 Ellipsoids collision with *Nr=1* (case B)

Starting from the same initial state, we now consider the aggregation between two equivalent ellipsoids (Eq.8), but with $N_r=1$. The figures 1B-6B must be compared with the figures 1A-6A corresponding to the reference case. First, we observe a good fit between all the corresponding curves, especially for the anisotropy factors (Figures 5-6), i.e. the pdf curves and their change with time. This ascertains some published conclusions by analysing the properties of the collision events between two given clusters [15]: the equivalent ellipsoid of the cluster represents well the cluster when considering any collision event. We also remark a slight difference between cases A and B: the catastrophic behaviour happens early for the case B. t_f value is equal to 0.13 (case A) versus 0.08 (case B).

One may also compare both cases A and B to the dynamics of shear aggregation of equivalent spheres, i.e. collision of two spheres leading to the sphere with the same matter volume. t_f value is now equal to 1.4 (not shown). Figure 8a represents the largest cluster size versus time. As expected, the size increase is exponential, but the time scale is much longer than the one for cases A and B. This behaviour is consistent with the compactness and the isotropy of the equivalent sphere, i.e. D_f=3, resulting in a much smaller value of the collision rate constant. Figure 8b represents the N-pdf for various times: the curves are similar to the ones of cases A and B, but with a more pronounced smoothness.

The gyration radius of the equivalent ellipsoid of a cluster consisting of N spheres with radius equal to one obeys the relation:

$$R_g = \sqrt{\left(a^2 + b^2 + c^2\right)/5} \qquad (15)$$

Considering the whole ellipsoid population, we observe that the gyration radius versus N obeys a power law as for fractal-like aggregates: $R_g = N^{1/1.75}$; therefore, the fractal dimension is equal to 1.75 whereas the prefactor is equal to 1.

3.3 Ellipsoids collision with *Nr=20000* (case C)

One could consider now the collision between averaged equivalent ellipsoids: the collision between two given ellipsoids is repeated N_r times and the averaged ellipsoid parameters are calculated following Eqs.4-5. The N_r value is taken equal to 20000 [15]. Figures 1C-6C must be compared with the figures corresponding to cases A and B. t_f value is again equal to 0.081. The data of case C concerning *N*-pdf, N_{max}, ϕ_{LC} and ϕ_{SLC} are very similar to those of case B. Concerning the anisotropy parameters, differences can be observed. *a/b* and *a/c*-pdf's are much narrower and less skewed in the case C, the density peak is around *a/b*=2.1 for case C whereas the one for case B is around 1.5. The locations of the peak for *a/c*-pdf are close to each other as cases B and C are compared. However the figure 9 shows that the mean values of the two anisotropy factors *a/b* and *a/c* over the population at a given time are close to each other. The average has been performed over the population with *N*>2; as the numerous monomers and dimers have constant anisotropy parameters, their contribution may mask the role of the larger particles.

The reason of the differences in the *a/b* and *a/c*-pdf's between cases B and C might be probably found in the averaging procedure performed in Eqs.4-5. The latter allows for a simple picture of the collision between two ellipsoids as depicted in Eq.7, but the effect of the ellipsoid random orientation is minimized.

To summarize, the deviations between the reference case and the two versions based on the ellipsoid representation of the cluster are the time scale slightly shorter for cases B and C and the *a/b*, *a/c*-pdf's narrower for case C.

Considering the whole ellipsoid population for case C, we observe that the gyration radius versus *N* obeys a power law as for fractal-like aggregates: $R_g = 1.02N^{1/1.76}$; therefore, the fractal dimension is equal to 1.76 whereas the prefactor is equal to 1.02.

3.4 Ellipsoids collision with approximate parameters (case D)

We have earlier presented an approximate expression for the collision kernel of two ellipsoids as well as the *a, b, c* parameters of the resulting equivalent ellipsoid [15]. This is a way to facilitate the implementation of the population balance and make the computation of the aggregation elementary act much faster. The ellipsoid parameters issued from the approximation are denoted by a_{app}, b_{app}, c_{app}; they are expressed as a function of $a_1, b_1, c_1, M_1, a_2, b_2, c_{2,} M_2$. The equations 16-18 recall the principles of the approximation: In order to take into consideration the physics of the collision, we start from an expression containing the diagonalized inertia tensor:

$$\underline{\underline{D_I}} = \underline{\underline{D_I^{(1)}}} + \underline{\underline{D_I^{(2)}}} + M_1 M_2 / \left(M_1 + M_2\right) \underline{\underline{f_{12}}} \qquad (16)$$

$\underline{\underline{f_{12}}}$ is a diagonal tensor the components of which are f_{bc}, f_{ac}, f_{ab}.

or

$$\begin{aligned} b_{app}^2 + c_{app}^2 &= \left(b_1^2 + c_1^2\right)\phi_1 + \left(b_2^2 + c_2^2\right)\phi_2 + 5\phi_1\phi_2 f_{bc} \\ a_{app}^2 + c_{app}^2 &= \left(a_1^2 + c_1^2\right)\phi_1 + \left(a_2^2 + c_2^2\right)\phi_2 + 5\phi_1\phi_2 f_{ac} \\ a_{app}^2 + b_{app}^2 &= \left(a_1^2 + b_1^2\right)\phi_1 + \left(a_2^2 + b_2^2\right)\phi_2 + 5\phi_1\phi_2 f_{ab} \end{aligned} \qquad (17a,b,c)$$

with $\phi_i = M_i / \left(M_1 + M_2\right)$. f_{bc}, f_{ac}, f_{ab} are to be determined. We have assumed that f_{bc}, f_{ac}, f_{ab} have a quadratic form in six variables:

$$\vec{u} = \left(u_1, u_2, u_3, u_4, u_5, u_6\right) = \left(a_1, b_1, c_1, a_2, b_2, c_2\right)$$

i.e. $f_{bc} = {}^T\vec{u}\mathbf{F_{bc}}\vec{u}$ (18)

The 6x6 matrix $\mathbf{F_{bc}}$ is symmetrical. $\mathbf{F_{bc}}$, $\mathbf{F_{ac}}$ and $\mathbf{F_{ab}}$ have been obtained from an optimization procedure using data issued from collision simulations. Knowing the range of values expected for $\vec{u}$ and ϕ_i (from case A), the data set used for optimization has been

slightly modified compared to [15]; therefore the fit has been improved. The three matrices are gathered in appendix.

As expected, the application of the approximate expressions leads to data close to the ones of case C (not shown in the paper). In order to take into account the above-mentioned highlights, the approximate expressions have been modified without loss of the computational performance and used as follows. Let us consider two real numbers *U* and *W*. We propose to consider the *a, b, c* ellipsoid parameters as random variables X_a, X_b, X_c . They obey the normal distribution with mean Wa_{app} , b_{app} or c_{app} and the standard deviation $\sigma_a = UWa_{app}$, $\sigma_b = Ub_{app}$ or $\sigma_c = Uc_{app}$. In order to slow down the aggregation and to represent the particles as slightly rounded, the *a* parameter will be modified as Wa_{app} (W<1). *U* quantifies the deviation of the actual resulting equivalent ellipsoid from the average one, due to the various relative orientation and positions of the colliding ellipsoids. *U* and *W* are fitting parameters. Figures 1D-6D represent the data corresponding to U=0.1 and W=0.985. The agreement with the data for the case A is very good. The sensitivity of the model with the *U* and *W* values is relatively low: U=[0.05-0.15] and W=[0.975-0.985] lead to very close data.

The choice of a normal distribution is justified by its simplicity and by the roughly Gaussian-shaped curve of the pdf's of ellipsoid parameters [15]; however, the relationship between the parameters of the two colliding ellipsoids and the pdf's of the resulting ellipsoid parameters seem to be very complicated [15]. It may be also underlined that the *W* parameter has so far not been related to physical parameters.

Considering the whole ellipsoid population, we observe that the gyration radius versus *N* obeys a power law as for fractal-like aggregates: $R_g = N^{1/1.8}$; therefore the fractal dimension is equal to 1.8 whereas the prefactor is equal to 1. It must be underlined that the increase of

the fractal dimension with time becomes much larger than the ones for cases A, B and C as t>0.1 (data not shown in the paper).

4. Discussion and conclusion

The data issued from this study will be discussed and compared to previous works of other investigators.

4.1. Relationship with previous works

We will only consider the works dedicated to theoretical considerations and simulations of pure shear aggregation; real clusters result from aggregation, restructuring and breakage. Pure shear aggregation is prevailing at the early phase of the process.

According to the literature, the D_f value for pure shear aggregation is within the range [1.8-2.0]. Whereas the fractal dimension for the reference case is within this range, these ones for cases B, C are slightly smaller than 1.8. This means that the porosity of the clusters increases more strongly with the primary particle number in the latter cases, and that an additional phenomenon will be needed for reducing the porosity of the ellipsoid resulting from the collision of two smaller ellipsoids. The fitting parameter W introduced in the approximate expressions plays this role in the modelling developed in the case D: this leads to a slight increase of the fractal dimension.

All the investigators agree that the prefactor is a function of the fractal dimension. Using such functions for D_f=1.9, for instance, Gmachowski [28] has found for k the value 0.93, Ehrl et al. [29] 0.92, Babick [7] 1.0, respectively. The prefactor values found in this work are therefore close to the published values.

When applying the Friedlander transformation to the N-pdf corresponding to the cases B, C and D, the transformed data poorly follow the expected self-preserving pdf, i.e. the one found in the case A (data not shown in the paper). This point will be discussed in the sub-section 4.2.

Regarding the anisotropy of clusters, the figure 9 indicates that the mean values of *a/b* and *a/c* are close to 2 and 3-3.5 respectively as already shown by Hentschel [9] and Torres [11].

Pranami et al. [13] have selected the two following shape anisotropy parameters $A_{13} = I_1 / I_3 = \left(a^2 + b^2\right) / \left(c^2 + b^2\right)$ and $A_{23} = I_2 / I_3 = \left(c^2 + a^2\right) / \left(c^2 + b^2\right)$ where I_1, I_2 and I_3 are the principal moments of inertia with $I_1 > I_2 > I_3$. They computed the A_{13}-pdf and A_{23}-pdf for different N values (N=64, 128, 256, 512) within the range of our data; Figures 10a-b show A_{13}-pdf and A_{23}-pdf for case D; these data agree well with frequency distributions shown in fig. 3 [13].

Frungieri and Vanni [12] define an aspect ratio as $AR = 2a / \left(b + c\right)$ where *a*, *b*, *c* are the parameters of the equivalent ellipsoid of the cluster and show that the *AR*-pdf is right skewed with a maximum value for *AR*=2 and a tail with values larger than 5. Figure 10c presents de *AR*-pdf for cases B and D; This can be compared to the *AR*-pdf for the population denoted by B in the figure 5.7 from Frungieri [8]; the data of Frungieri are closer to the data from case B than those of case D. However, all the distributions have a similar pattern.

4.2. Improvement based on physical principles

The deviation between the reference case (A) and cases B, C concerns mainly the fractal dimension and the aggregation time (and rate). The empirical approach used in case D in order to improve the modelling is based on shortening the largest semi-axis of the equivalent ellipsoid. The benefit of such approach is the simplicity. The drawback is its artificial character. However the physical reason of the deviation is the possible interpenetration of the colliding sphere clusters which is not taken into account during the collision of equivalent ellipsoids. Thus, the following improvement is proposed: The equivalent ellipsoid consists of a hard core and a penetrable shell with the thickness dependent on the permeability κ of the ellipsoid. The contact point between the two colliding ellipsoids is at the level of the two core

boundaries. Several authors have evaluated the penetration length of a cluster (see Potanin [10], Veerapaneni et al. [30], Neale et al. [31]). They are in agreement, proposing the relation $L = 2\sqrt{\kappa}$ (valid if the fractal dimension is higher than 1.8 in a 3-D space). The permeability κ of a set of spheres with radius *R* may be expressed as:

$$\kappa = \frac{2R^2}{9f}\frac{H(f)}{E} \tag{19}$$

where *H(f)* and *E* are respectively the Happel's function [32] and the shielding factor [33]:

$$H(f) = \frac{3 - 4.5f^{1/3} + 4.5f^{5/3} - 3f^2}{3 + 2f^{5/3}} \tag{20a}$$

$$E = 1 - 0.6e^{-10f} \tag{20b}$$

*f i*s the volume fraction of matter inside the porous medium, i.e. the cluster ($f = N/(abc)$). Note that the ellipsoid is considered homogeneous with a constant density.

Then the distance (C_1C_2) between the centres of the two equivalent ellipsoids is reduced due to the reciprocal penetration of the two equivalent ellipsoids:

$$(C_1C_2) = (C_1C_2)_0 - 2\left(\sqrt{\kappa_1} + \sqrt{\kappa_2}\right) \tag{21}$$

The interpenetration leads to a densification that is implicitly handled by the model.

The supplementary material contains the result of the implementation of Eqs. 19-21 into the modelling of ellipsoid collisions. The implementation is straightforward for the cases B and C. Concerning the approximate expression (case D), we propose to modify only the part of Eq.16 involving the inter-centre distance of the two colliding ellipsoids. Two ways were tested:

i) Changing the vector $\vec{u} = (a_1, b_1, c_1, a_2, b_2, c_2)$ in $\underline{\underline{f_{12}}}$ by

$\vec{u} = \left(a_1 - 2\sqrt{\kappa_1}, b_1 - 2\sqrt{\kappa_1}, c_1 - 2\sqrt{\kappa_1}, a_2 - 2\sqrt{\kappa_2}, b_2 - 2\sqrt{\kappa_2}, c_2 - 2\sqrt{\kappa_2}\right)$, or

ii) Multiplying $\underline{\underline{f_{12}}}$ by the scalar $\left(1-2\left(\sqrt{\kappa_1}+\sqrt{\kappa_2}\right)/d\right)^2$ where d is an estimate of $\left(C_1C_2\right)_0$. d is chosen as a function of the gyration radii of the colliding ellipsoids: $d = R_{g,1} + R_{g,2}$. The exponent 2 comes from the dependence of $\vec{A}$ in Eq.2.

This physical modelling replaces the introduction and the use of the empirical parameter *W*; it is equivalent to set the *W* value at 1. The value of *U* is maintained at 0.1 because this parameter is not concerned by the above physical modelling. The effects of these two ways of correcting on the data reported in the figures 1-6 are very close. Only the second one is shown in the figures 1D-6D. Moreover, the fractal dimension is within the range [1.9; 2.0] whereas the prefactor is within the range [0.9; 1]. It can be seen that the agreement between cases A, B and D is very good. The figures 7A-D in the supplementary material show the *N*-pdf after the Friedlander's transform. It can be seen that all the size distributions fall on the self-preserving curve. The agreement between cases A, B and D is again validated.

The both empirical and physical corrections for approximate expressions (Eqs.17a,b,c) lead to similar data (figures 1-6). The use of these approximate expressions (case D) reduces the computing time of PBE solving by a factor of 50 compared to the case C. The benefit is therefore significant. The physical correction based on the cluster permeability is satisfactory when considering a scientific approach. However, the introduction of the permeability of the two colliding particles in Eqs.17a,b,c makes non quadratic the $\underline{\underline{f_{12}}}$ and $\underline{\underline{D_I}}$ expressions with respect to $\left(a_1,b_1,c_1,a_2,b_2,c_2\right)$; As a consequence, deriving, for instance, $\left(a_2,b_2,c_2\right)$ knowing $\left(a_1,b_1,c_1\right)$ and $\left(a_{app},b_{app},c_{app}\right)$ may become difficult, as

required for the PBE solving. This should be easier when only correcting the a_{app} value by the fitting factor *W*.

As a conclusion, we have shown that the sphere clusters can be successfully replaced by their equivalent ellipsoids when studying aggregation. This modelling can be illustrated by the scheme in Figure 11. At time t_1 of the aggregation process, the suspension contains primary particles and clusters; the suspension evolves then thanks to binary collisions which lead to larger clusters at time t_2. At time t_1, the population may be described as a population of ellipsoids defined from their inertia tensor. If this ellipsoid set undergoes collisions obeying the aggregation act considered in this paper until t_2, then the population of ellipsoids at t_2 models correctly the population of clusters at t_2. The proof of the agreement includes the comparison of size distributions, anisotropy parameter distributions, values of the fractal dimension and the prefactor of the fractal law, self-similarity behaviors. Moreover, the approximate expressions previously proposed for computing the ellipsoid parameters of the resulting particle after collision allow for faster and representative Monte Carlo simulations of the aggregation process of the particle population. As the interpenetration of colliding clusters is considered the modelling of aggregation is improved.

This modelling dedicated to the pure aggregation is only valid for the first stage of the entire aggregation process. Restructuring and fragmentation have not been considered in this work as they occur later on. The latter are related to the deformation of the object, i.e. cluster or ellipsoid. We expect that the use of ellipsoids instead of clusters facilitates the modelling of these new phenomena. This study is in progress.

References

[1] M. Elimelech, J. Gregory, X. Jia, R. Williams, “Particle deposition & aggregation”, Butterworth-Heinemann, 1995

[2] S. Kumar and H. Briesen, 4th International Conference on Population Balance Modeling, Chemical Engineering Science 70(2012)

[3] G.E. Schroeder-Turk, W. Mickel, S.C. Kapfer, F.M. Schaller, B. Breidenbach, D. Hug, K. Mecke, “Minkowski tensors of anisotropic spatial structure“,arXiv: 1009.2340v5 6 Aug 2013

[4] C.H. Arns, M.A. Knackstedt, K.R. Mecke, “Characterisation of irregular spatial structures by parallel sets and integral geometric measures”, Colloids and Surfaces A: Physicochemical and Engineering Aspects, 241 (2004) 351-372

[5] M. Essadki, F. Drui, S. Chaisemartin, A. Larat, T. Ménard, M. Massot, « Statistical modeling of gas-liquid interface using geometrical variables : toward a unified description of the disperse and separated phase flows », https://hal.archives-ouvertes.fr/hal-01615076

[6] D.A. Drew, “Evolution of geometric statistics”, SIAM J. Appl. Math. 50(1990)649-666

[7] F. Babick, “Suspensions of colloidal particles and aggregates”, Particle Technology Series, Springer, 20, 2016

[8] G. Frungieri, “A novel Monte Carlo – Discrete Element Method approach for the micro-mechanics of colloidal suspensions”, PhD dissertation, Politecnico di Torino, 2018

[9] H.G.E. Hentschel, “The structure and fractal dimension of cluster-cluster aggregates” in “Kinetics of aggregation and gelation” edited by F. Family and D.P. Landau, North-Holland, 1984

[10] A.A. Potanin, “On the mechanism of aggregation in the shear flow of suspensions”, J. of Colloid and Interface Science 145 (1991) 140-157

[11] F.E. Torres, W.B. Russel, W.R. Schowalter, “Simulations of coagulation in viscous flows”, J. of Colloid and Interface Science 145 (1991) 51-73

[12] G. Frungieri, M. Vanni, “Shear‐induced aggregation of colloidal particles: A comparison between two different approaches to the modelling of colloidal interactions”, the Canadian Journal of Chemical Engineering, 95(2017)1768-1780

[13] G. Pranami, M.H. Lamm, R.D. Vigil, “Molecular dynamics simulation of fractal aggregate diffusion”, Physical Review E82(2010) 051402

[14] F. Gruy, “Inertia tensor as morphological descriptor for aggregation dynamics”, Colloids and Surfaces A: Physicochemical and Engineering Aspects, 482(2015)154-164.

[15] F.Gruy, P. Nortier « Statistics about collisions of ellipsoids under shear flow » Colloids and Surfaces A: Physicochemical and Engineering Aspects, 558(2018)250-262

[16] L. Gmachowski, “Estimation of the dynamic size of fractal aggregates”, Colloids and Surfaces A: Physicochemical and Engineering Aspects, 170(2000)209-216.

[17] L. Landau, E. Lifchitz, Mécanique, Editions MIR, Moscou, 1969

[18] D.T. Gillepsie, « An exact method for numerically simulating the stochastic coalescence process in a cloud”, J. of the Atmospheric Sciences, (1975)1977-1989

[19] M. Smith, T. Matsoukas, “Constant-number Monte Carlo simulation of population balances”, Chemical Engineering Science, 53(1998)1777-1786

[20] C.W. Ormel, M. Spaans, A.G.G.M. Tielens, “Dust coagulation in protoplanetary disks: porosity matters”, ArXiv:astro-ph/0610030v1 2 Oct 2006.

[21] H. Tanaka, K. Nakazawa, “Validity of the statistical coagulation equation and runaway growth of protoplanetary”, Icarus, 107(1994)404-412.

[22] V. Oles, “Shear-Induced Aggregation and Breakup of Polystyrene Latex Particles”, J. of Colloid and Interface Science, 154(1992) 351-358

[23] L. Alfonso, G.B. Raga, D. Baumgardner, “The validity of the kinetic collection equation revisited”, Atmospheric Chemistry and Physics, European Geosciences Union, 8(2008)969-982

[24] L. Alfonso, G.B. Raga, D. Baumgardner, “The validity of the kinetic collection equation revisited – Part 3: Sol-gel transition under turbulent conditions”, Atmospheric Chemistry and Physics, 13(2013)521-529

[25] A. Cameirao, R. David, F. Espitalier, F. Gruy, “Effect of precipitation conditions on the morphology of strontium molybdate agglomerates”, J. of Crystal Growth 310 (2008) 4152–4162

[26] S.K. Friedlander, C.S. Wang, “The self-Preserving particle size distribution for coagulation by Brownian motion”, J. of Colloid and Interface Science 22(1966)126-132

[27] L. Gmachowski, “ Mechanism of shear aggregation”, Water. Res. 29(1995)1815-1820

[28] L. Gmachowski, “ Hydrodynamics of aggregated media”, J. of Colloid and Interface Science 178(1996)80–86

[29] L. Ehrl, M. Soos, M. Lattuada, “Generation and Geometrical Analysis of Dense Clusters with Variable Fractal Dimension”. J. Phys. Chem. B, 113(2009)10587–10599

[30] S. Veerapaneni, M.R. Wiesner, “Hydrodynamics of fractal aggregates with radially varying permeability”, J. of Colloid and Interface Science 177 (1996) 45-57

[31] G. Neale, N. Epstein, W. Nader, “Creeping flow relative to permeable sphere”, Chemical Engineering Science 28 (1973) 1865-1874

[32] J. Happel, H. Brenner, “low Reynolds number Hydrodynamics”, Englewood Cliffs, N.J. : Prentice-Hall, 1965 ; J. Happel, “Viscous flow in multiparticle systems: slow motion of fluids relative to beds of spherical particles”, AIChE. Journal, 4(1958)197-201

[33] M. Vanni, " Creeping flow over spherical permeable aggregates", Chemical Engineering Science, 55(2000)685-698

Appendix: 6x6 matrices for approximate expressions (Eqs.17a,b,c; Eq.18)

$\mathbf{F_{bc}}$

-0.1165	0.1803	0.1852	0.1655	-0.0073	-0.0037
0.1803	-0.2208	-0.0356	-0.0073	-0.0818	-0.0580
0.1852	-0.0356	-0.3227	-0.0037	-0.0580	0.0543
0.1655	-0.0073	-0.0037	-0.1165	0.1803	0.1852
-0.0073	-0.0818	-0.0580	0.1803	-0.2208	-0.0356
-0.0037	-0.0580	0.0543	0.1852	-0.0356	-0.3227

$\mathbf{F_{ac}}$

0.6011	-0.3102	-0.3578	-0.0995	0.3017	0.1147
-0.3102	0.5141	0.4383	0.3017	0.0969	0.0763
-0.3578	0.4383	0.3442	0.1147	0.0763	0.0173
-0.0995	0.3017	0.1147	0.6011	-0.3102	-0.3578
0.3017	0.0969	0.0763	-0.3102	0.5141	0.4383
0.1147	0.0763	0.0173	-0.3578	0.4383	0.3442

$\mathbf{F_{ab}}$

0.4664	-0.1066	-0.0582	0.0587	0.1380	0.1656
-0.1066	0.4751	-0.2575	0.1380	0.0563	0.0910
-0.0582	-0.2575	0.9031	0.1656	0.0910	0.0958
0.0587	0.1380	0.1656	0.4664	-0.1066	-0.0582
0.1380	0.0563	0.0910	-0.1066	0.4751	-0.2575
0.1656	0.0910	0.0958	-0.0582	-0.2575	0.9031

List of figures

Figures 1-6: Color (N_t) black (100); red (300); green (500); blue (1000); magenta (2000); cyan (3000)

Case A, B: N_a=10; Case C: N_a=1; Case D: N_a=5

Figure 1A: N-pdf for various times (repeated twice).

Figure 1B, 1C, 1D: N-pdf for various times.

Figure 2A: N-pdf for various times (repeated twice).

Figure 2B, 2C, 2D: N-pdf for various times.

Figure 3A, 3B, 3C, 3D: N_{max} versus time

Figure 4A, 4B, 4C, 4D: mass fraction of the largest cluster (*) and the second largest cluster (o) versus time.

Figure 5A: a/b-pdf for various times (repeated twice).

Figure 5B, 5C, 5D: a/b-pdf for various times.

Figure 6A: a/c-pdf for various times (repeated twice).

Figure 6B, 6C, 6D: a/c-pdf for various times.

Figure 7a: gyration radius R_g versus N for t=0.136 (case A)

Figure 7b: self-preserving population density; $n(N,t)<N>$ against $N/<N>$ for various times.

Figure 8: shear aggregation of equivalent spheres. Color (N_t) black (1000); red (2000); green (5000); blue (7500); magenta (10000)

a. N_{max} versus time for two realizations; b: N-pdf for various times.

Figure 9: mean anisotropy parameters versus time

triangle: a/b; circle: a/c empty (Case A) full (Case C)

Figure 10a: A_{13}-pdf for comparison of case D (N>4) with Pranami et al. [13] . Case D: solid lines; Pranami's work: full circles.

Figure 10b: A_{23}-pdf for comparison of case D (N>4) with Pranami et al. [13]. Case D: solid lines; Pranami's work: full circles.

Figure 10c: AR-pdf for comparison of cases B and D (N>4) with Frungieri (fig.5.7 [8]). Cases B and D: solid lines; Frungieri's work: full circles.

Figure 11: cluster aggregation versus ellipsoid aggregation

Figure1A

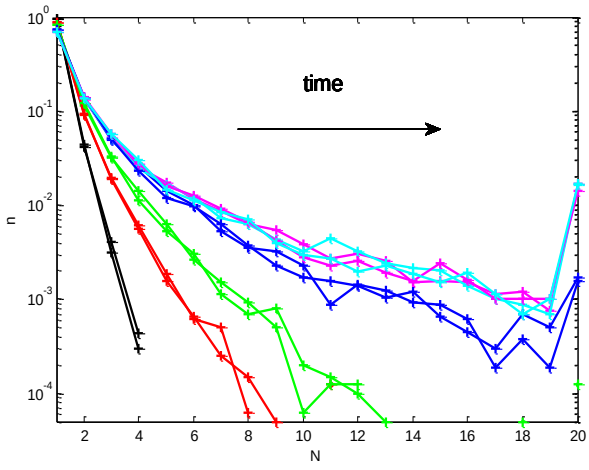

Figure1B

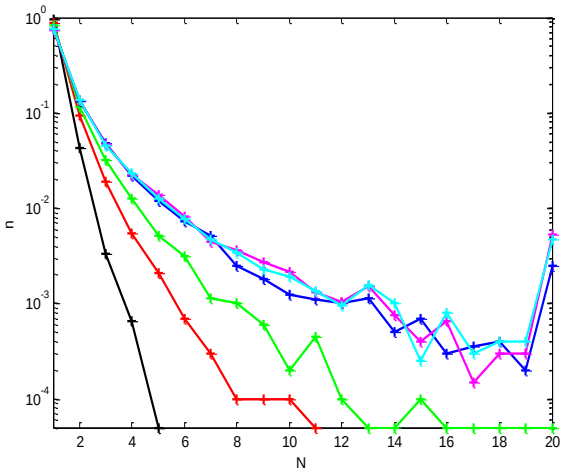

Figure1C

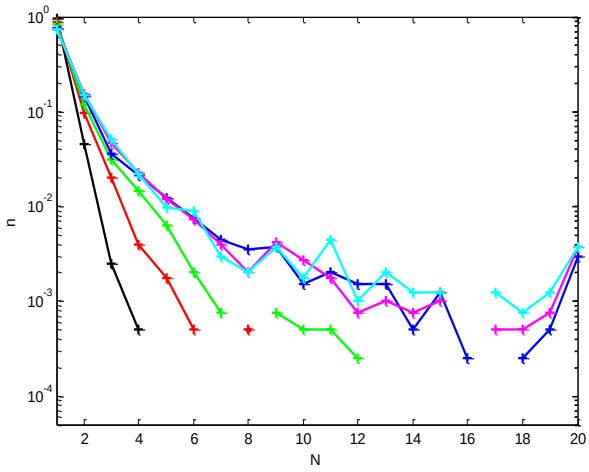

Figure1D

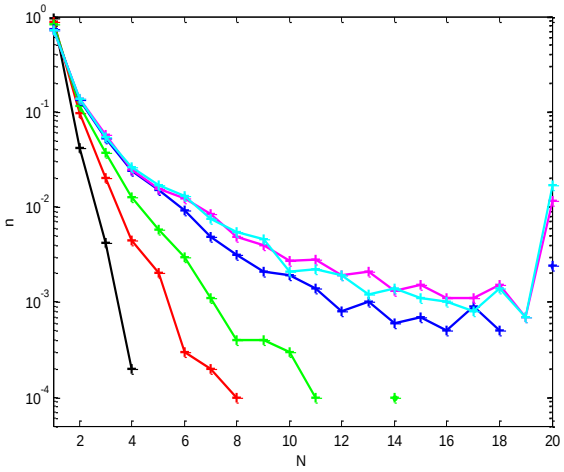

Figure2A

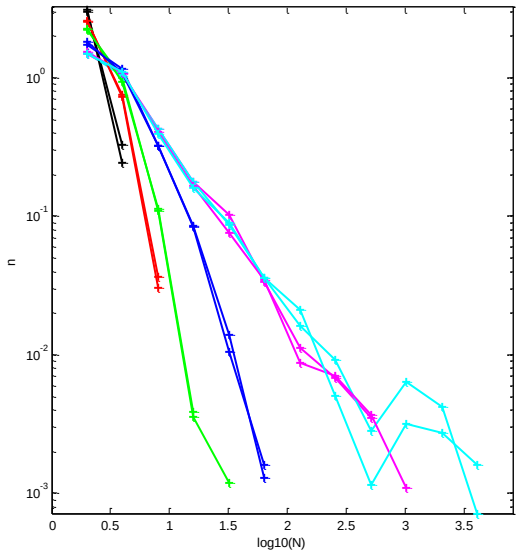

Figure2B

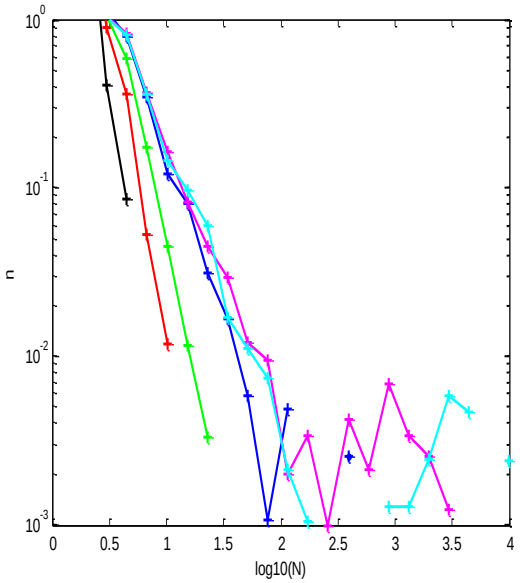

Figure2C

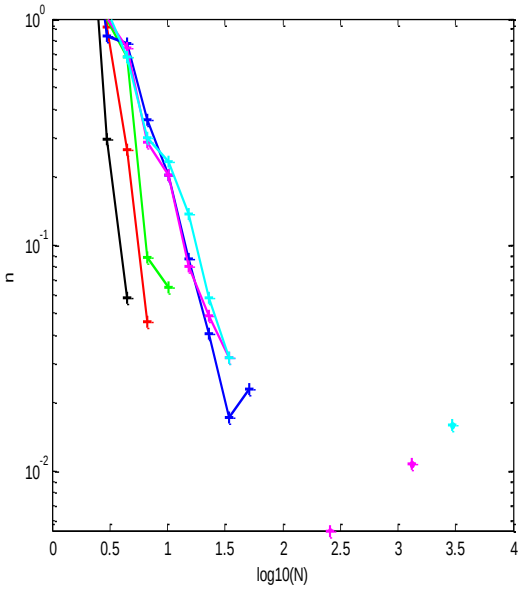

Figure2D

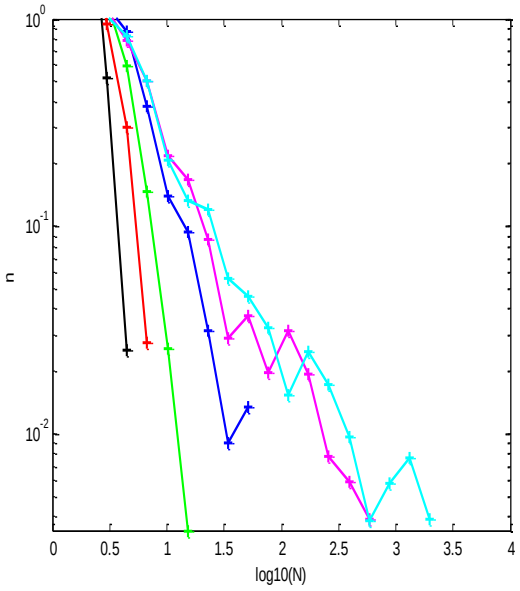

Figure3A

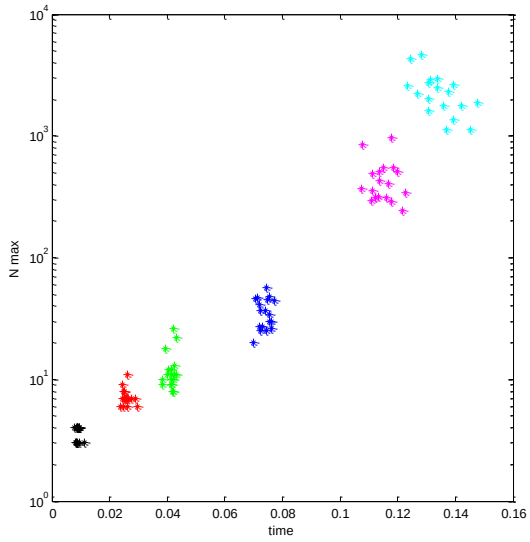

Figure3B

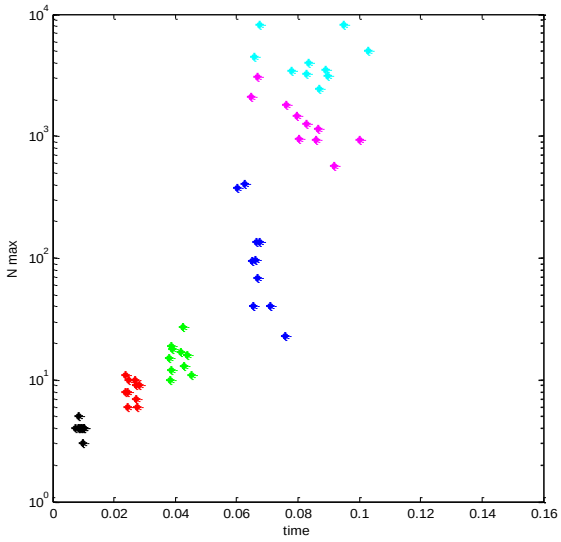

Figure3C

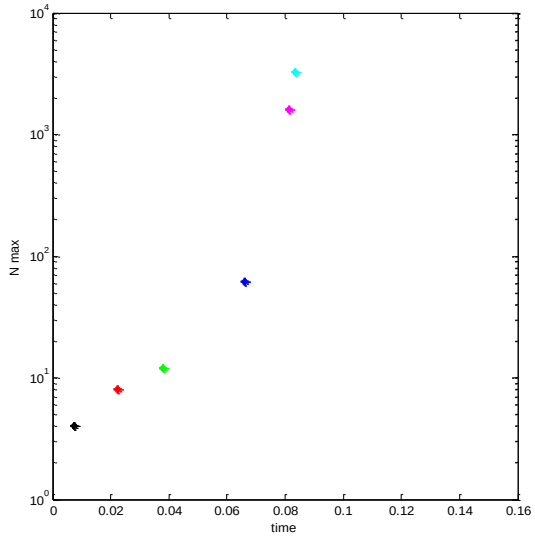

Figure3D

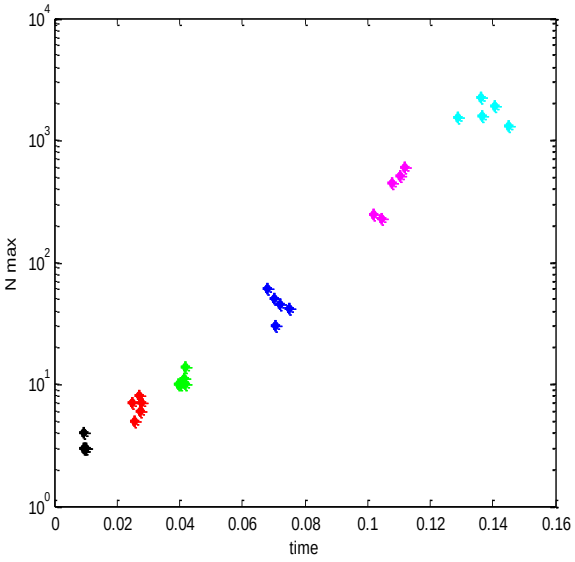

Figure4A

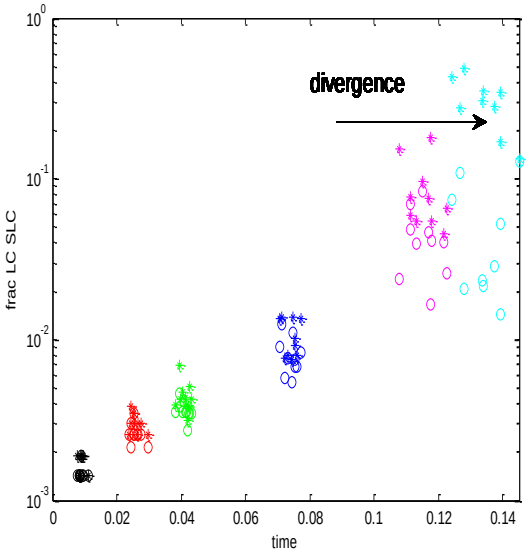

Figure4B

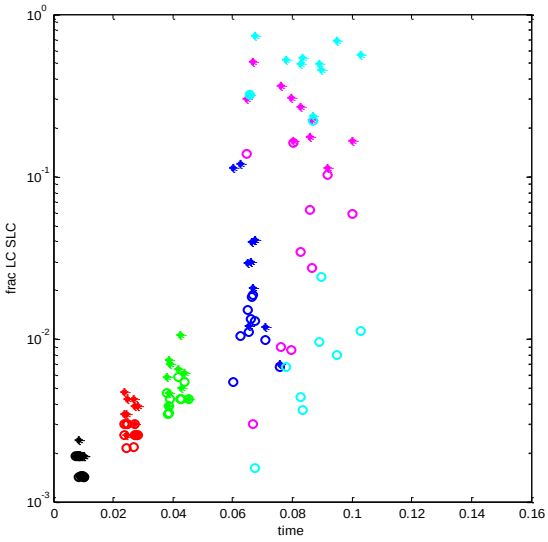

Figure4C

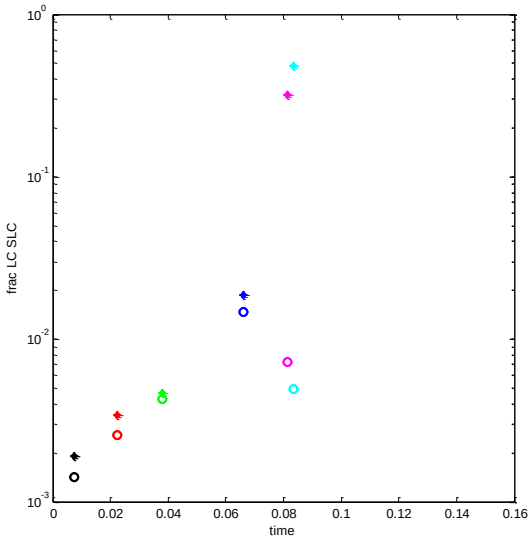

Figure4D

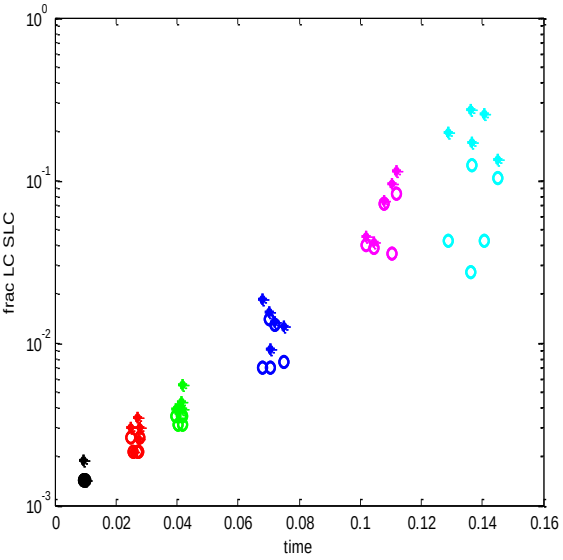

Figure5A

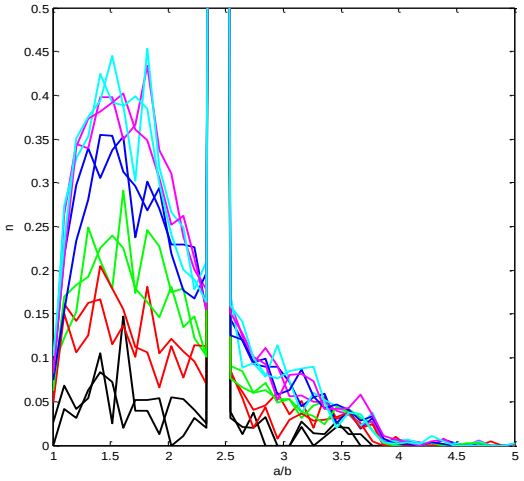

Figure5B

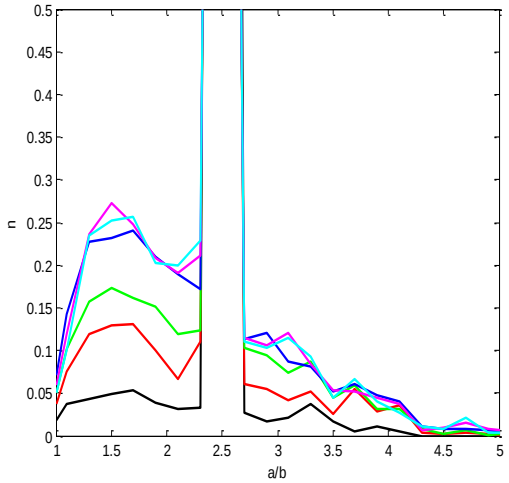

Figure5C

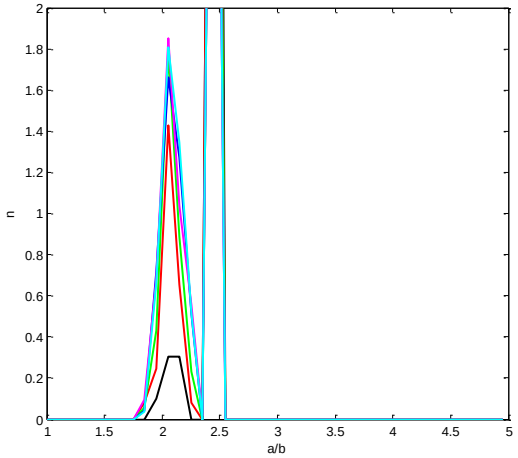

Figure5D

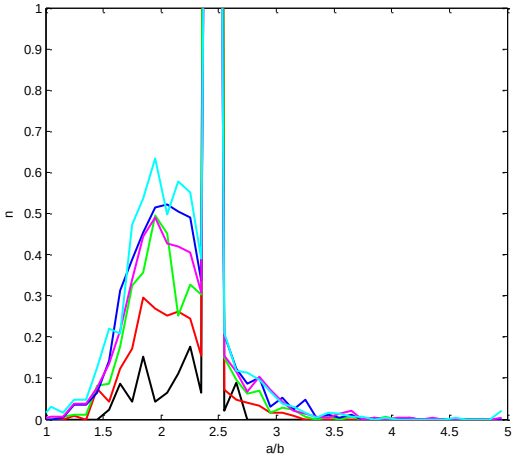

Figure6A

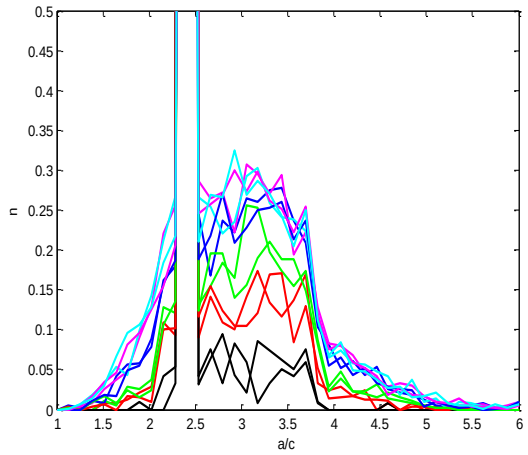

Figure6B

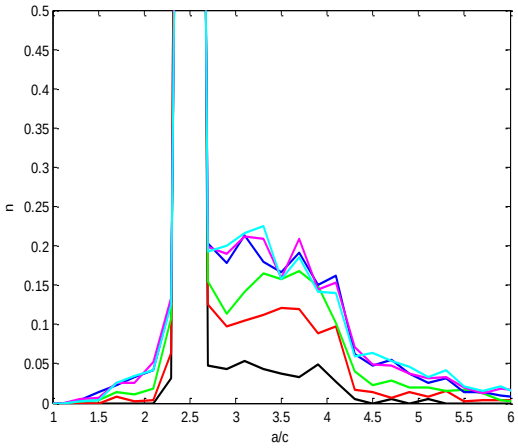

Figure6C

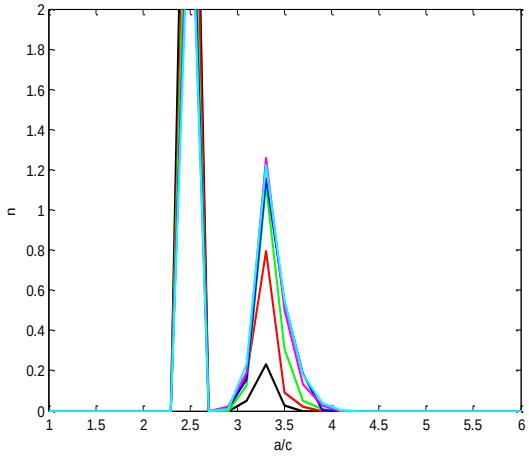

Figure6D

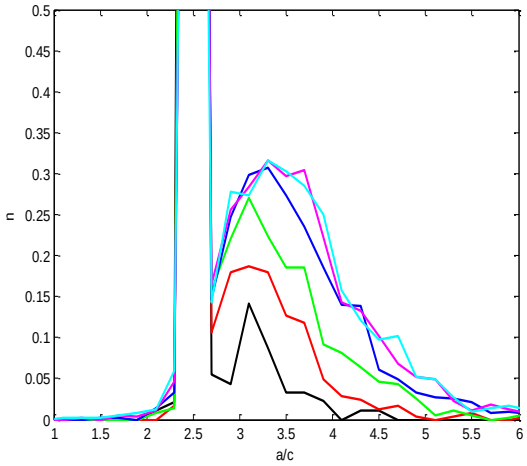

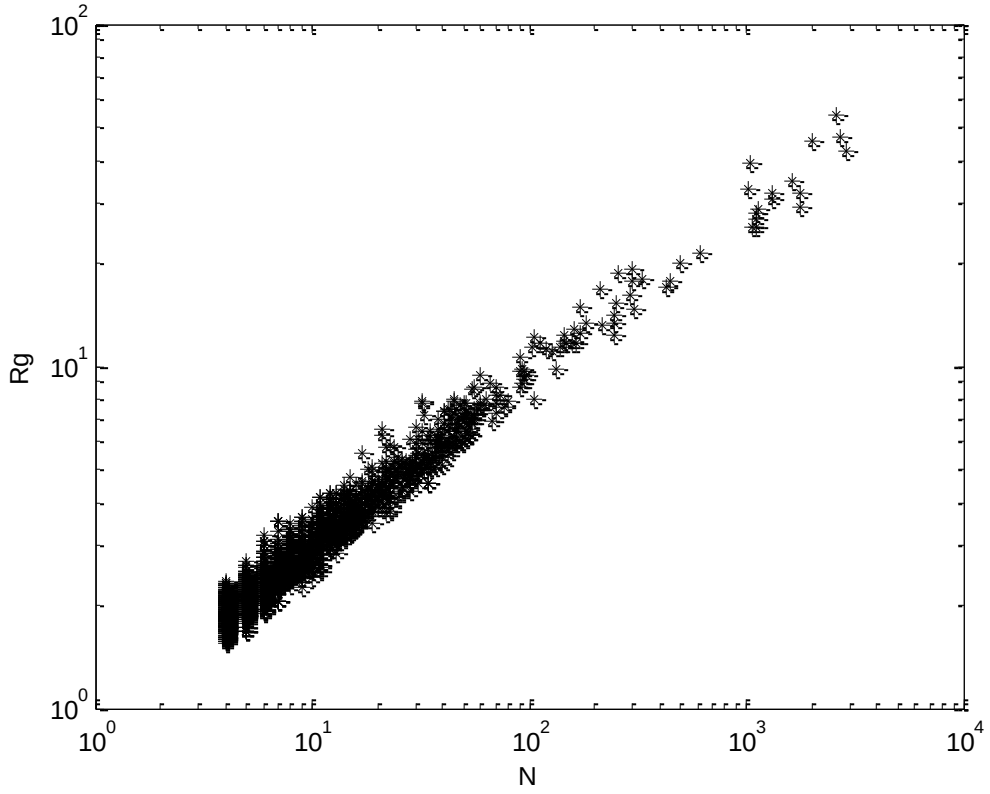

Figure 7a

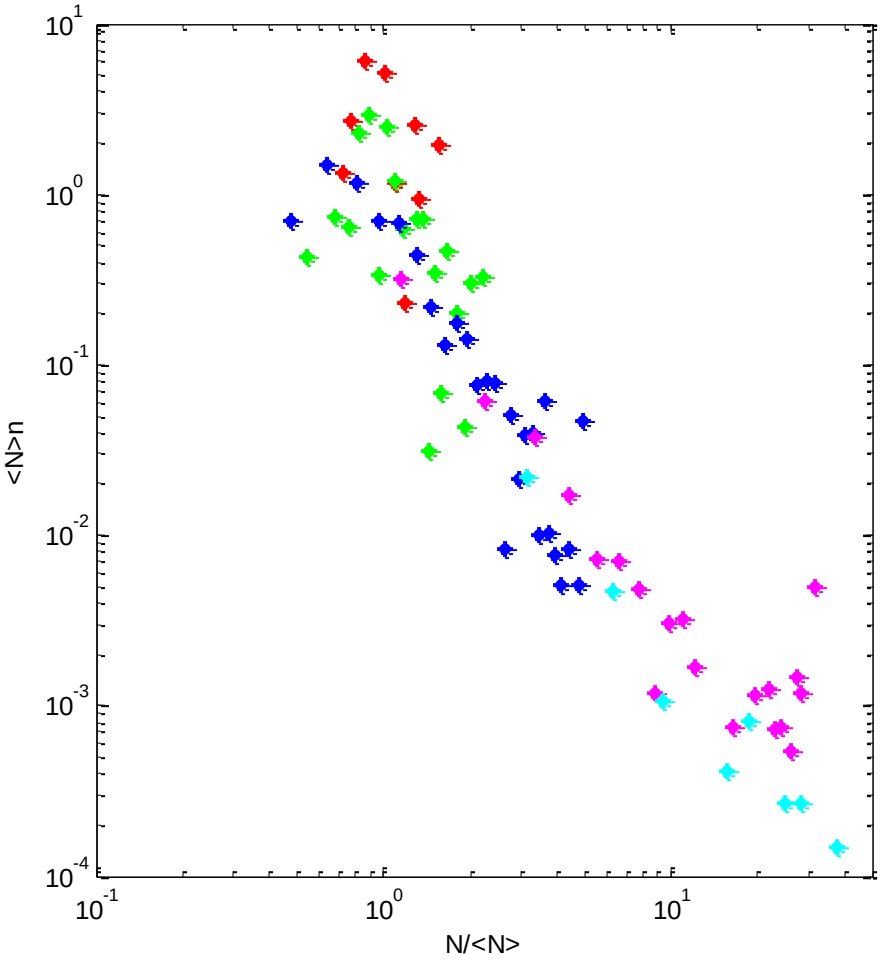

Figure 7b

a

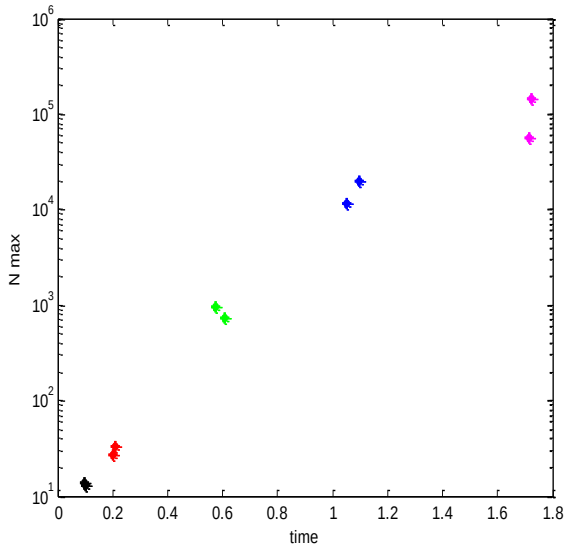

b

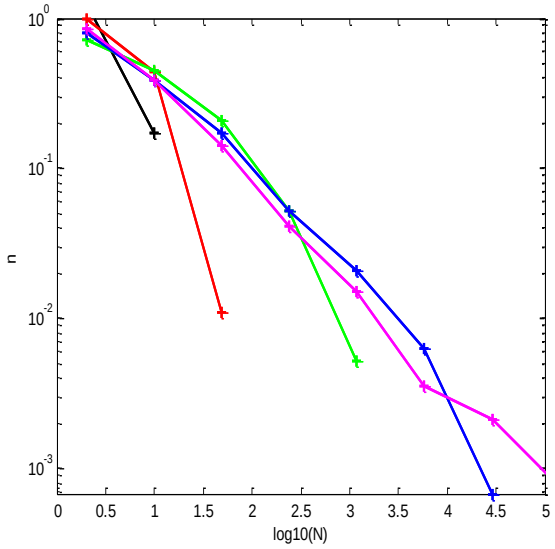

Figure 8 a,b

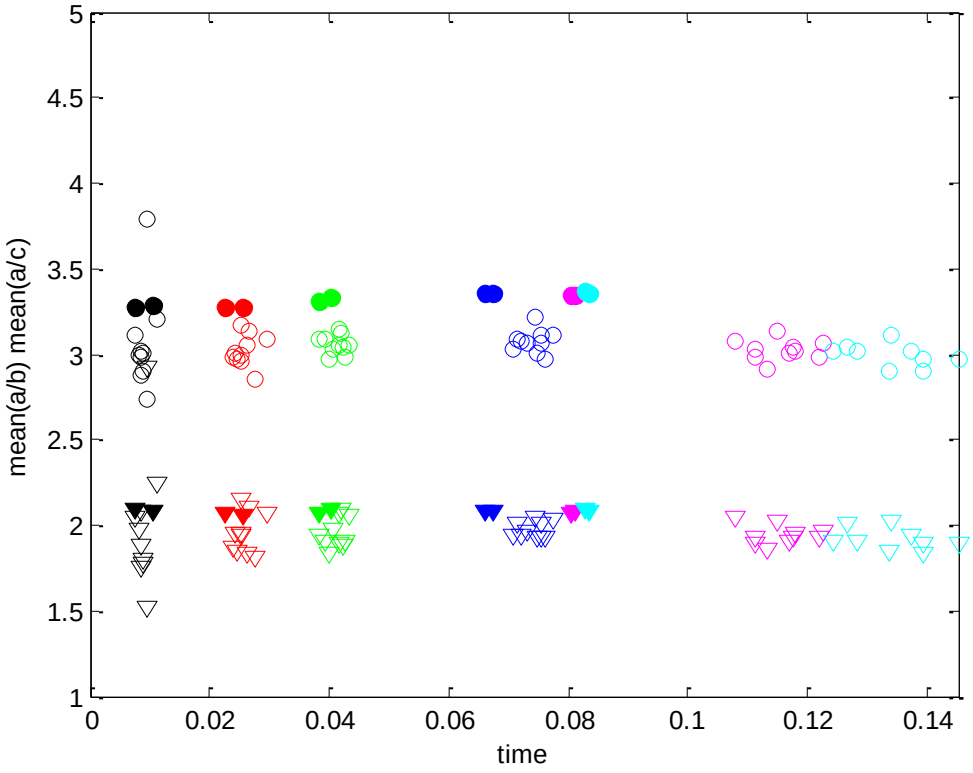
mean(a/b) mean(a/c)
time
5
4.5
4
3.5
3
2.5
2
1.5
1
0
0.02
0.04
0.06
0.08
0.1
0.12
0.14

Figure 9

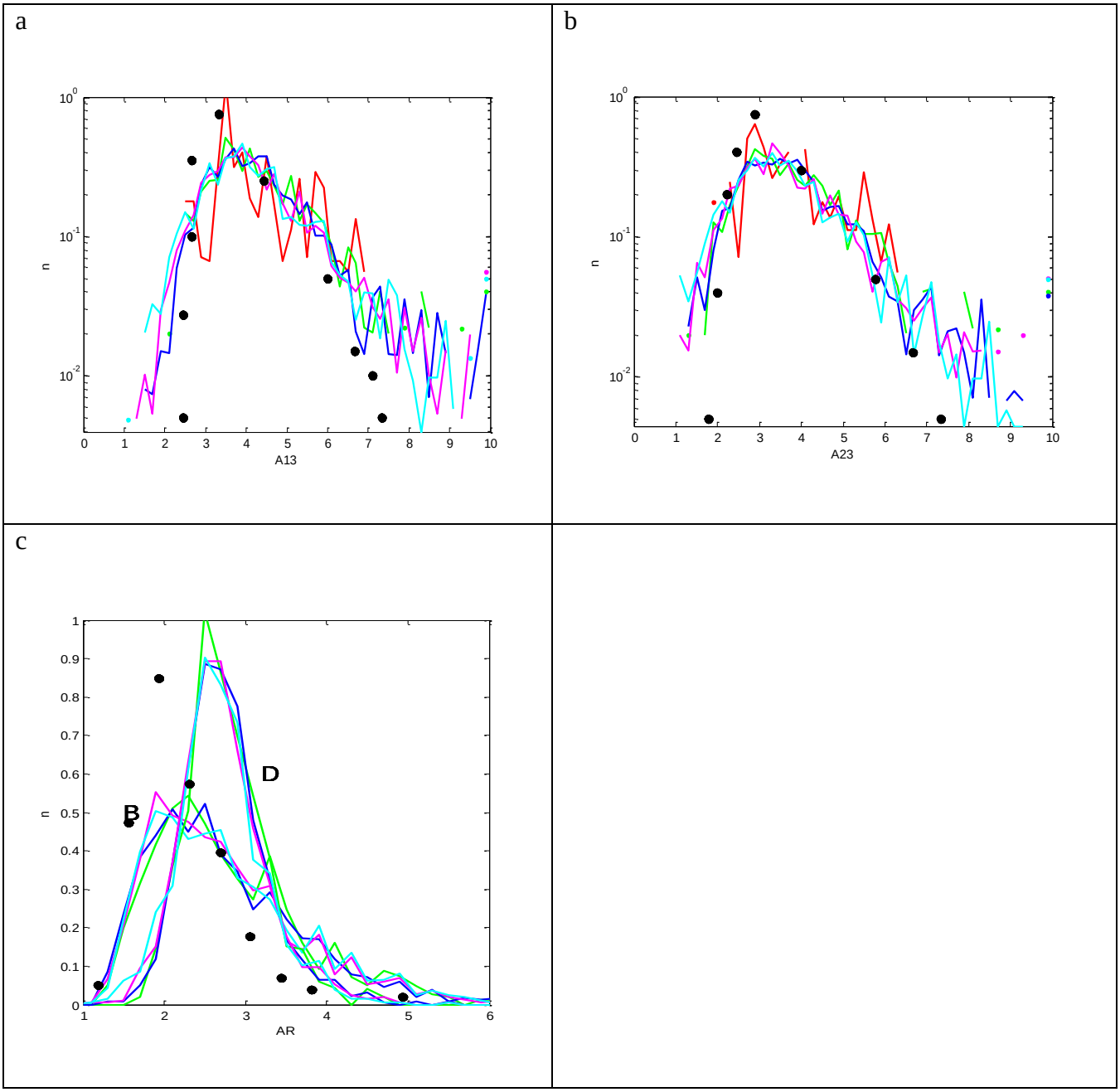

Figure 10 a,b,c

Figure 11

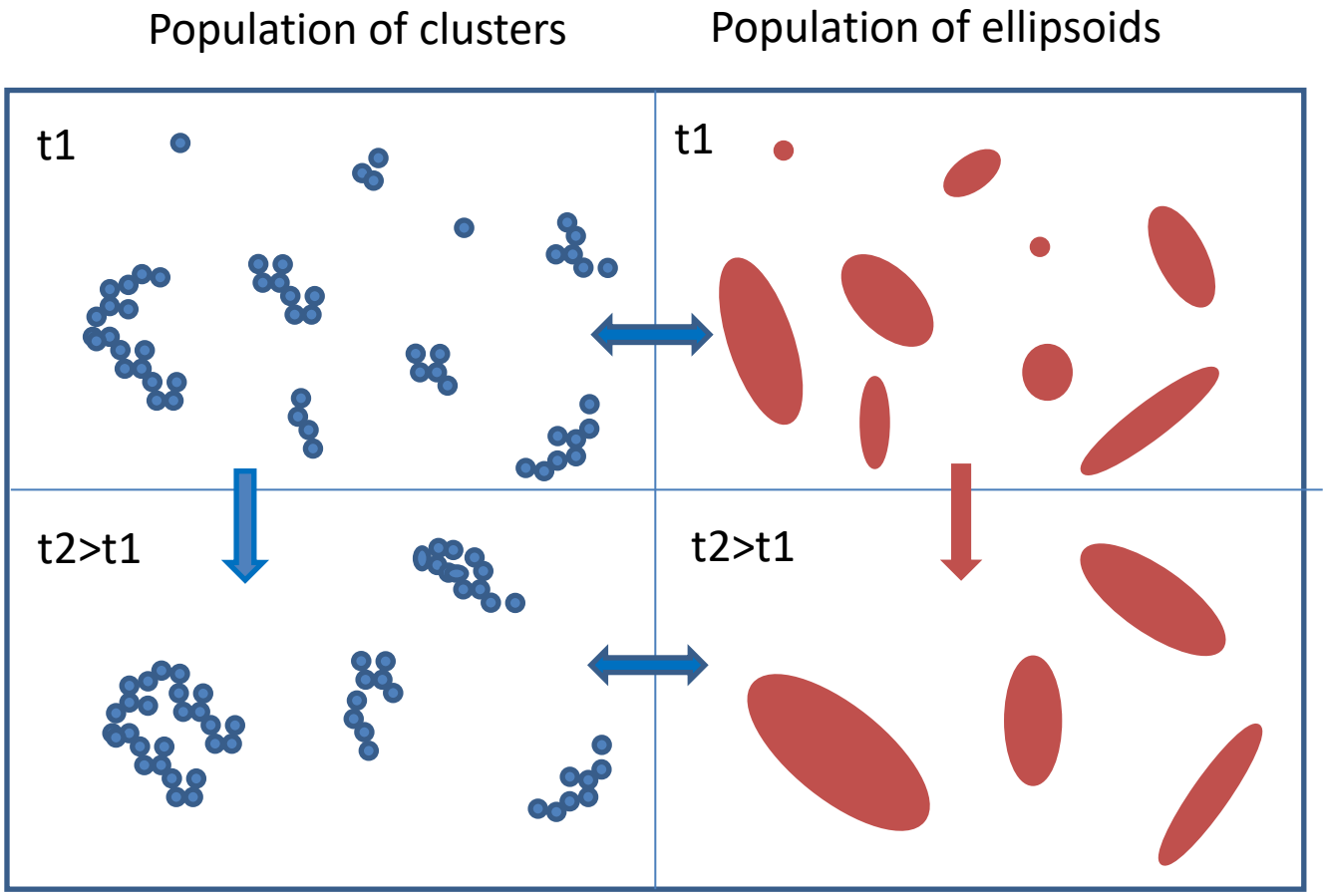
Population of clusters
Population of ellipsoids
t1
t1
t2>t1
t2>t1

Supplementary Material

Effect of the permeability of the equivalent ellipsoids on the shear-aggregation dynamics (cases B, C and D); case A: reference case

List of figures

Figures 1-7: Color (N_t) black (100); red (300); green (500); blue (1000); magenta (2000); cyan (3000)

Case A, B, D: N_a=10; Case C: N_a=2

Figure 1A: N-pdf for various times (repeated twice).

Figure 1B, 1C, 1D: N-pdf for various times.

Figure 2A: N-pdf for various times (repeated twice).

Figure 2B, 2C, 2D: N-pdf for various times.

Figure 3A, 3B, 3C, 3D: N_{max} versus time

Figure 4A, 4B, 4C, 4D: mass fraction of the largest cluster (*) and the second largest cluster (o) versus time.

Figure 5A: a/b-pdf for various times (repeated twice).

Figure 5B, 5C, 5D: a/b-pdf for various times.

Figure 6A: a/c-pdf for various times (repeated twice).

Figure 6B, 6C, 6D: a/c-pdf for various times.

Figure 7A, 7B, 7C, 7D: self-preserving N-pdf: N-pdf for various times as $n(N,t) < N >$ versus $N / < N >$.

Figure1A

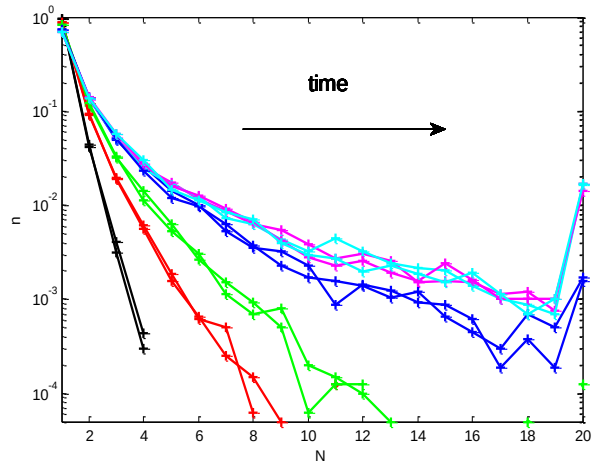

Figure1B

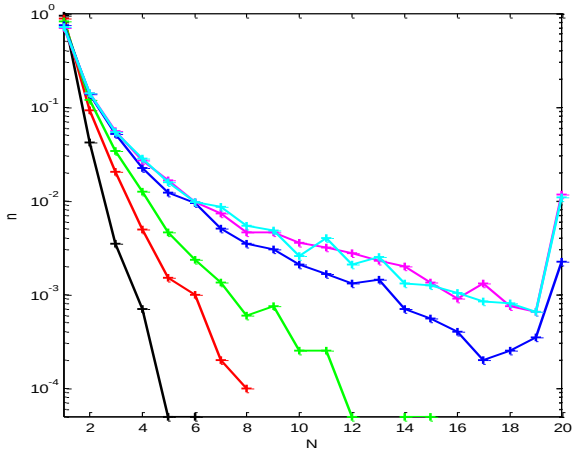

Figure1C

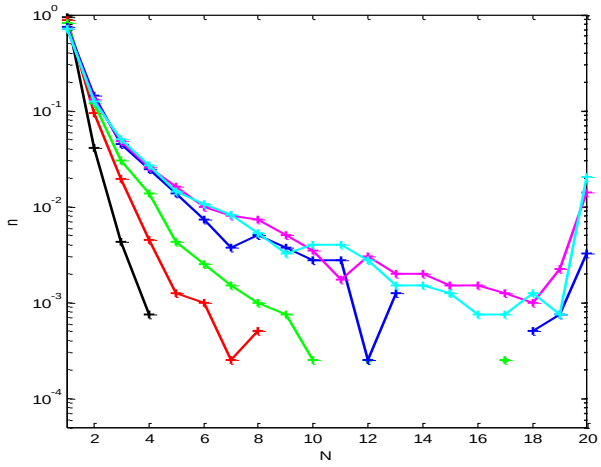

Figure1D

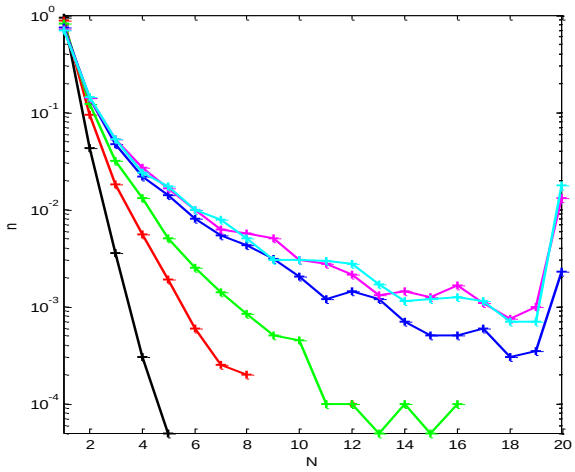

Figure2A

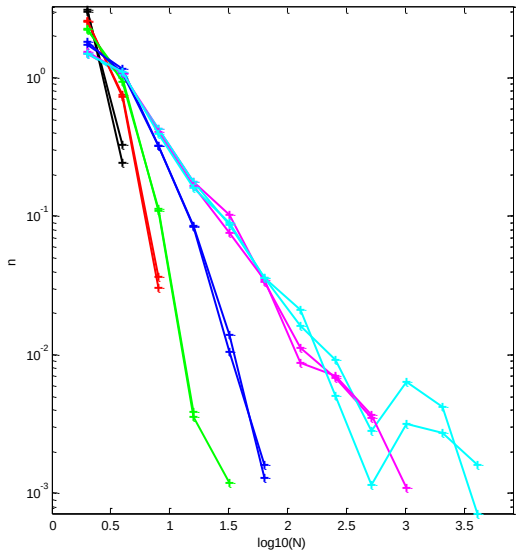

Figure2B

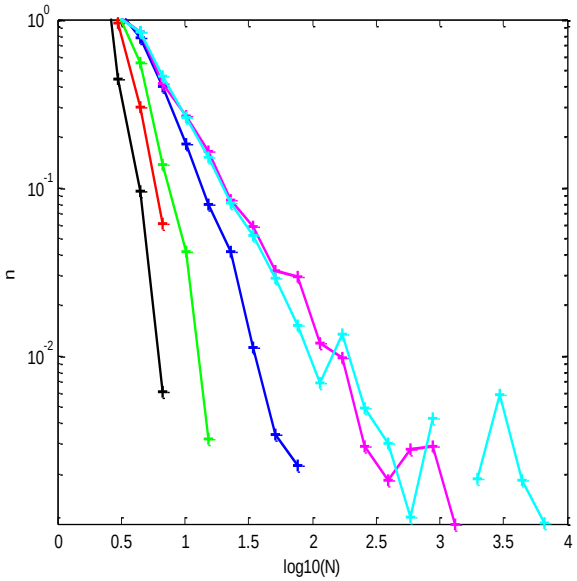

Figure2C

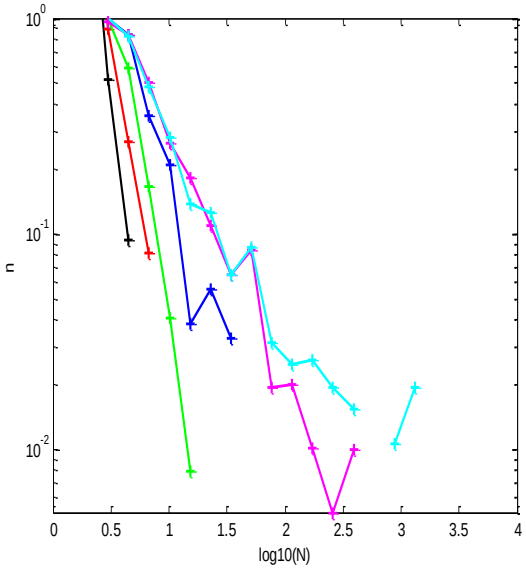

Figure2D

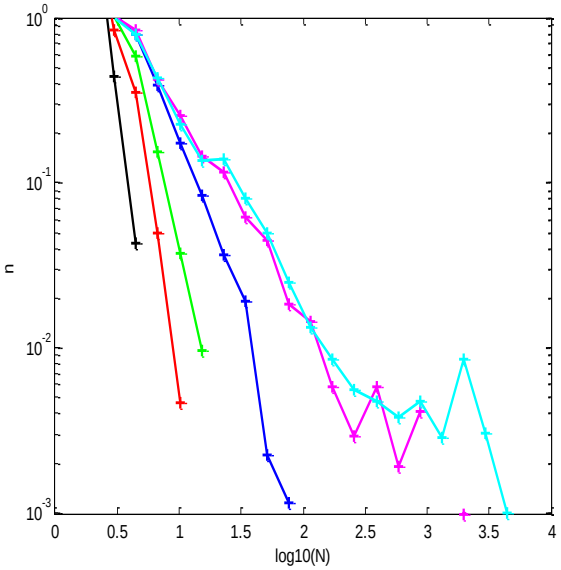

Figure3A

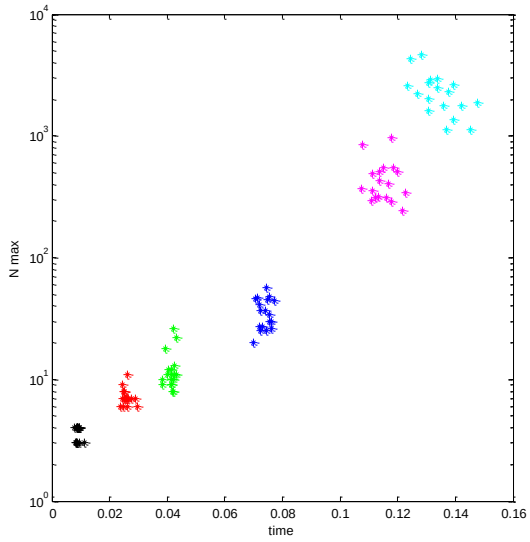

Figure3B

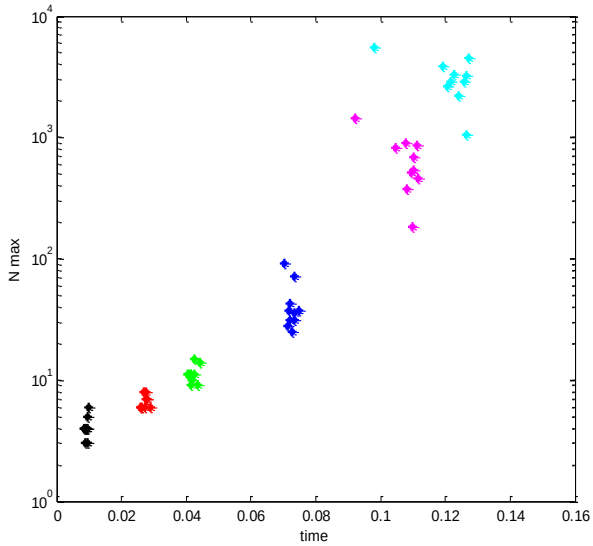

Figure3C

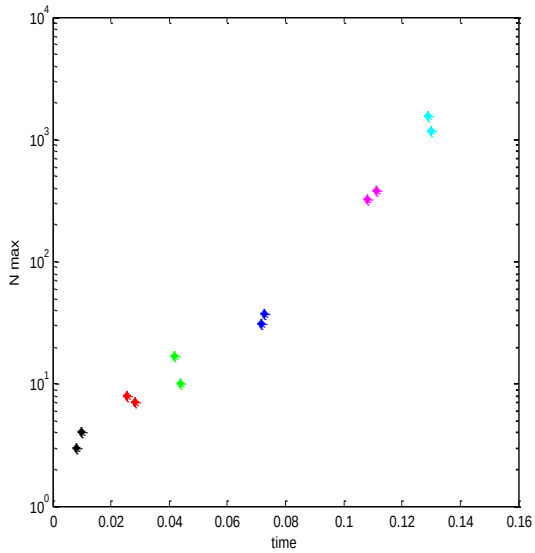

Figure3D

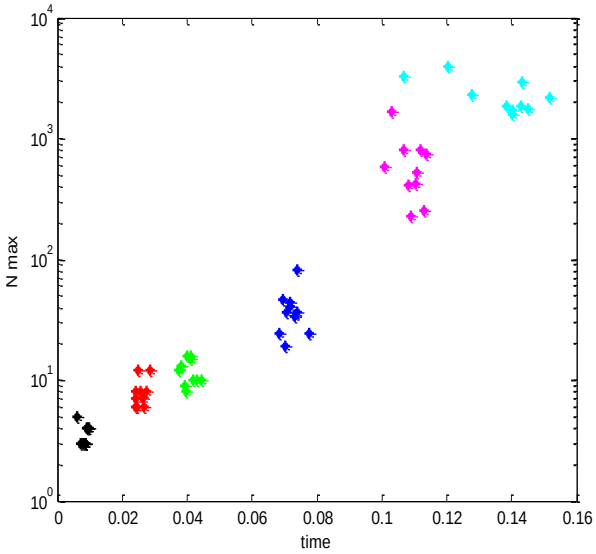

Figure4A

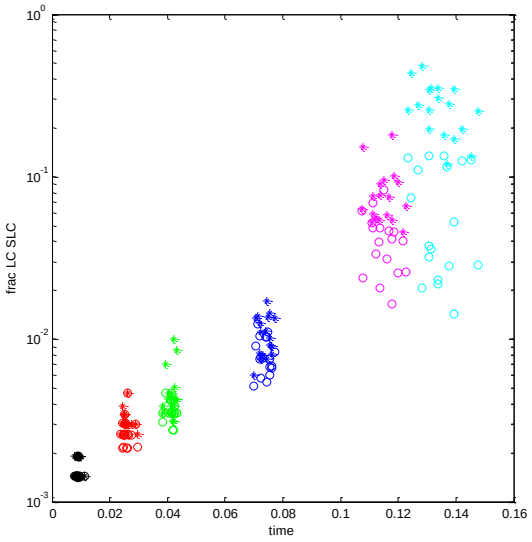

Figure4B

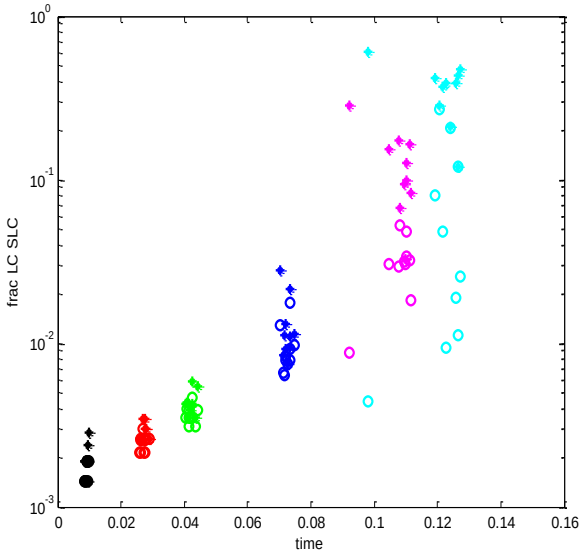

Figure4C

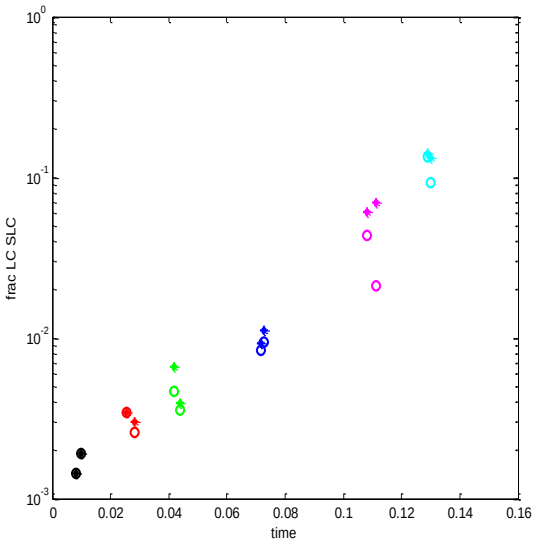

Figure4D

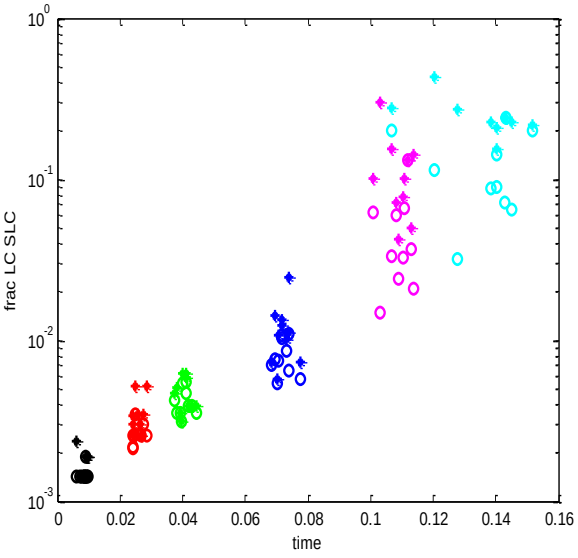

Figure5A

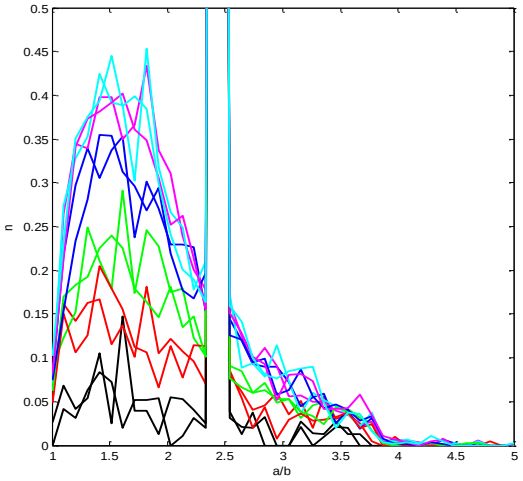

Figure5B

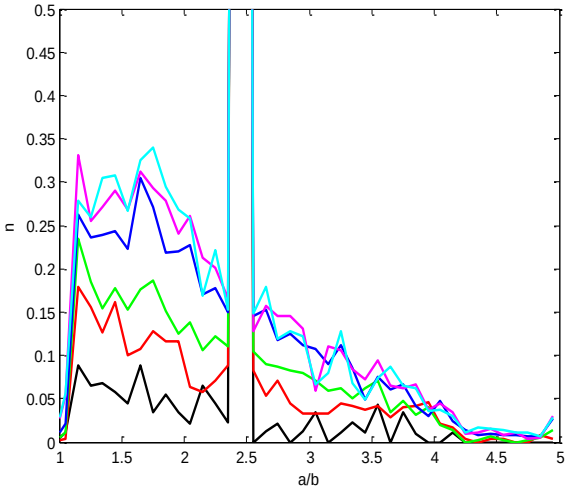

Figure5C

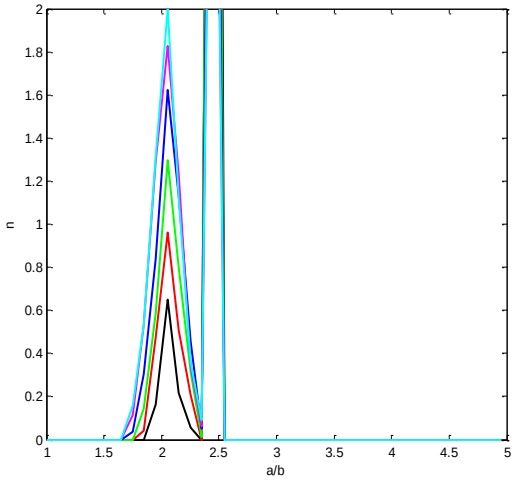

Figure5D

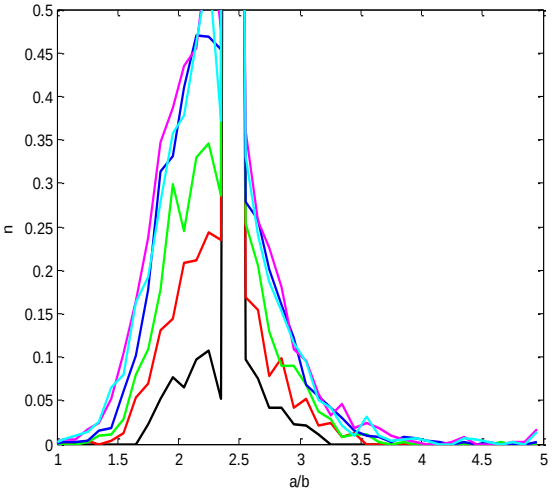

Figure6A

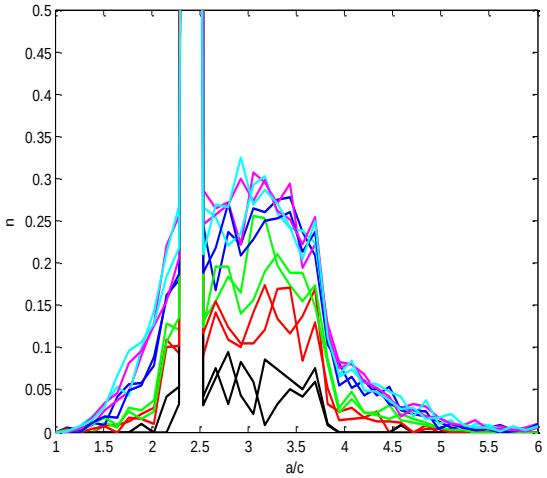

Figure6B

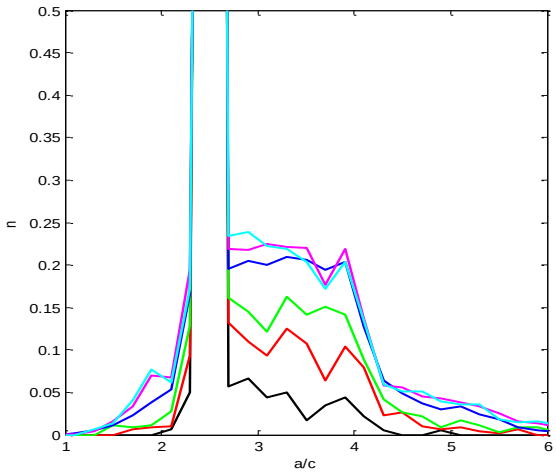

Figure6C

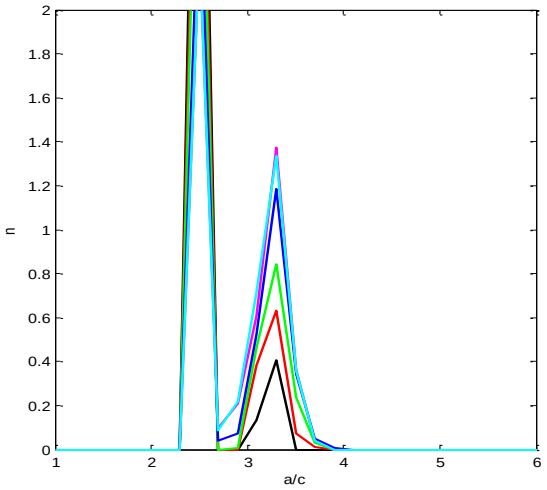

Figure6D

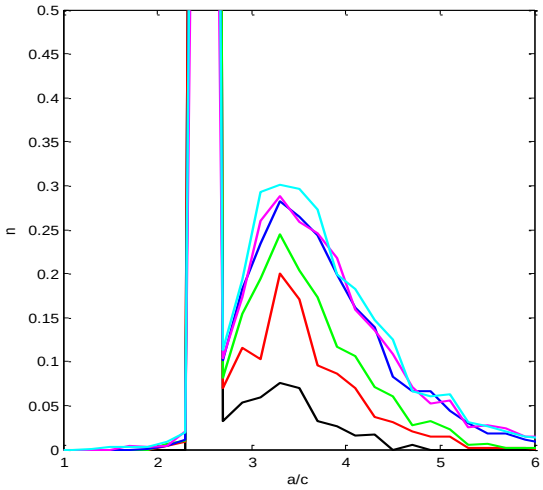

Figure7A

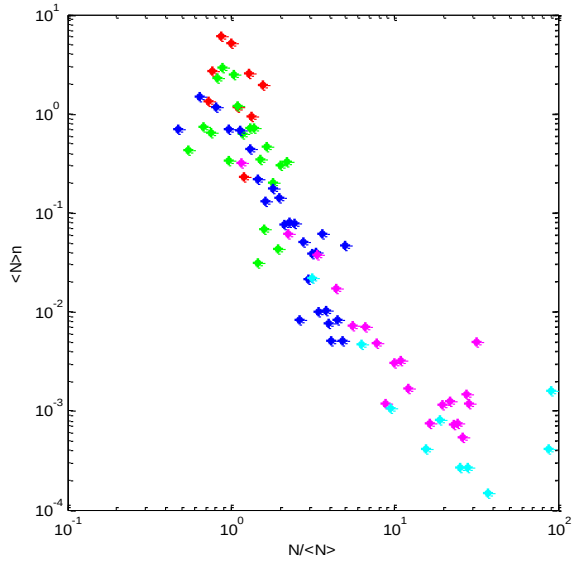

Figure7B

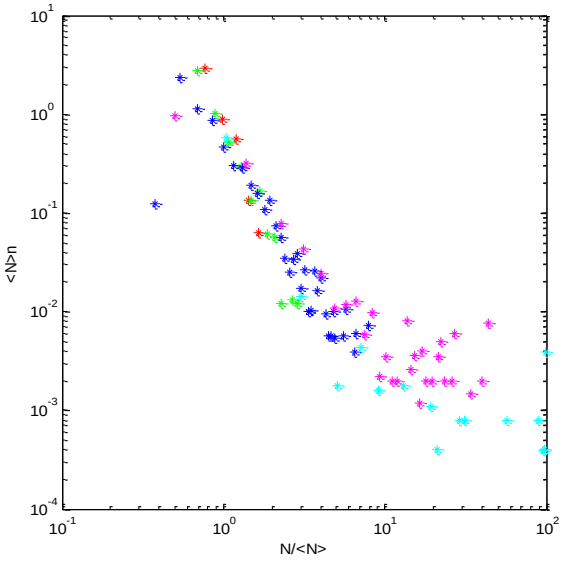

Figure7C

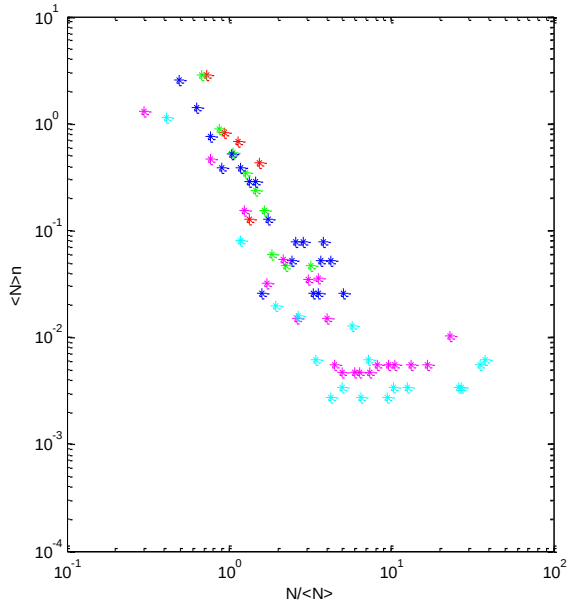

Figure7D

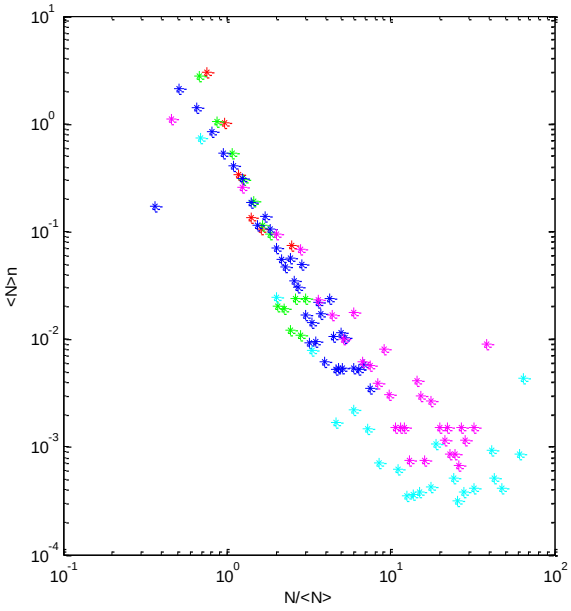

t	0	0.009	0.026	0.0415	0.074	0.116	0.136
<N>	1	1.05	1.16	1.28	1.66	2.85	4.1

Table 1: mean N value versus time (case A)

t	0.026	0.041	0.074	0.116	0.136
k	0.876	0.887	0.916	0.932	0.941
D_f	1.943	1.88	1.94	1.975	2.00

Table 2: k and D_f versus time t (case A)